Meteorology and Atmospheric Physics (2023) 135:5
https://doi.org/10.1007/s00703-022-00941-2

ORIGINAL PAPER

Impact of sea-breeze circulation on the characteristics of convective thunderstorms over southeast India

B. Revanth Reddy[1] · C. V. Srinivas[1,2] · B. Venkatraman[1,2]

Received: 5 June 2022 / Accepted: 8 November 2022 / Published online: 28 November 2022

Abstract

The impact of Sea-breeze circulation on the convective thunderstorms over the southeast coast of Tamilnadu, India is studied using the Weather Research and Forecasting (WRF) model. High-resolution (2-km) simulations are conducted with WRF for two severe thunderstorm events on 24 April 2015 in summer 22 July 2015 in the southwest monsoon. Surface observations of Automated Weather Stations (AWS), gridded accumulated rainfall, radiosonde, and Doppler Weather Radar (DWR) reflectivity products are used for model evaluation. Simulations indicated that the moisture convergence in the sea breeze frontal zone and the presence of lower atmospheric wind shear during sea breeze are the main factors for the initiation of deep convection and intensification of the thunderstorms. Simulations reveal that the thunderstorms developed in summer are more intensive due to more intense and deep-sea breeze circulation cells developing under weak synoptic flow during summer compared to monsoon. Results show that simulated summer thunderstorms are associated with higher CAPE, lower CIN, stronger vertical motion in association with a stronger convergence, higher buoyancy and larger low-level wind shear and lower upper air shear compared to the monsoon thunderstorms. The presence of stronger lower atmospheric wind shear during summer sea-breeze favours the development of strong and deep convection compared to the monsoon season. Results also showed a simulation of more solid hydrometeors (ice, snow and graupel) due to intense convection in summer compared to the monsoon season.

1 Introduction

Thunderstorms are mesoscale systems characterized by gusty winds, thunder, lightning and intense rain. They can have a severe impact on the infrastructure, agriculture and life. Several studies have been conducted in the past on the development mechanism and characteristics of thunderstorms (Manohar et al. 1999; Basu and Mondal 2002; Kandalgaonkar et al. 2005; Tyagi 2007; Allen et al. 2011; Bhardwaj and Singh 2018; among others) due to their significant impact on local weather conditions. These storms develop on a spatial scale varying from a few kilometers to a few hundred kilometers, and with a temporal scale ranging from a few minutes to a few hours. The height of the cloud base in a thunderstorm begins from 450 to 600 m above the earth's surface, and the cloud tops have been observed to reach 12–15 km height in tropical regions (Lutgens and Tarbuck 1982). High moisture availability, atmospheric instability, vertical wind shear and a lifting mechanism are the necessary conditions for the development of thunderstorms (Chaudhari et al. 2010; Sahu et al. 2020; Sindhu and Bhat 2021). Thermodynamical changes and/or dynamical forcing initiates the formation of the storm by providing the thrust to lift the air mass. Strong surface heating along with high moisture provides high thermodynamic instability, whereas orographic lifting or air mass convergence at lower levels provide a favorable dynamical forcing. The combined influence of these two factors facilitates the rapid development of thunderstorms (Haklander and Van Delden 2003; Manzato 2005). The latent heating in the clouds provides the necessary buoyancy to the air parcel that supports deep convection (Wallace and Hobbs 1977).

The accurate prediction of thunderstorm formation, location, and intensity is vital to protect lives, mitigate damage to property and agricultural resources, and for safe and efficient aviation operations (Tyagi 2007). Apart from conventional

Responsible Editor: Clemens Simmer, Ph.D.

✉ C. V. Srinivas
venkatasrinivasc@yahoo.com; cvsri@igcar.gov.in

[1] Homi Bhabha National Institute, Mumbai 400094, India

[2] Environmental Assessment Division, Indira Gandhi Centre for Atomic Research, Kalpakkam 603102, India

thermodynamic stability methodology, there has been an increase in the use of high-resolution mesoscale weather prediction models for the simulation and prediction of severe local convective storms. Several studies have been carried out for the simulation of pre-monsoon thunderstorms over the Indian region (Litta and Mohanty 2008; Srivastava et al. 2008, 2010; Litta et al. 2012; Fadnavis et al. 2014; Prasad et al. 2014; Singh et al. 2015; Dinesh et al. 2016; Srikanth et al. 2016a; Osuri et al. 2017; Leena et al. 2019; Sisodiya et al. 2019) using different mesoscale models. These studies have reported successful simulations of different features such as the timing of storm development, structure, evolution and rainfall patterns. Most of these studies have been focused primarily on inland thunderstorms.

The development of sea breeze during the warm season in different coastal parts of India is known to affect the local weather (Suresh and Bhatnagar 2005) and has been shown to play an important role in air pollution dispersion (Srikanth et al. 2016b, 2018). Previous studies over southern peninsular India also show that sea breeze is the predominant mesoscale circulation affecting the regional weather and is the chief source of moisture for the convective thunderstorms over this region (Suresh and Bhatnagar 2005; Srinivas et al. 2006; Simpson et al. 2007, 2008; Rani et al. 2010; Chen et al. 2014; Poljak et al. 2014; Bhate et al. 2016). Sea breeze influences the local winds and rainfall during summer and southwest monsoon (Suresh and Bhatnagar 2005; Simpson et al. 2007, 2008). Observational studies over southeast India (Suresh and Bhatnagar 2005; Rani et al. 2010; Suresh 2012) suggest that thunderstorms in this region are often associated with sea breeze which transports a large amount of moisture, causes convergence inland and triggers the development of convection and rainfall. Numerical modelling studies suggest that the sea breeze progresses deep inland during warm seasons and generates thunderstorms inland as far as 150 km from the coast (Suresh and Bhatnagar 2005; Simpson et al. 2008; Rani et al. 2010; Suresh 2012; Bhate et al. 2016).The characteristics of the sea breeze circulation in terms of its intensity, inland intrusion, frontal convergence etc., varies according to topography, land -sea temperature gradient and synoptic scale circulations (Azorín-Molina and Chen 2009; Muppa et al. 2012; Arrillaga et al. 2016; Calmet et al. 2017).

The sea breeze varies in different seasons in southeast India in terms of its onset time, horizontal intrusion and intensity (Suresh and Bhatnagar 2005; Rani et al. 2010; Suresh 2012). When the atmosphere is conditionally unstable, the forced ascent of air in the lower regions over a sea breeze front can trigger deep convection (Kingsmill 1995). Therefore, the inland propagation of sea breeze front controls the formation of convective thunderstorms, their location and intensity, etc. by the convergence of the marine and the continental airmasses in coastal regions (Fankhauser et al. 1995; Kingsmill 1995; Azorín-Molina et al. 2014; Comin et al. 2015). Further, this influence of sea breeze circulation on the deep convection and initiation of storm development is more probable under favorable synoptic conditions i.e., when synoptic scale forcing is negligible. The variation of synoptic wind over southern peninsular India i.e., strong south-westerlies during monsoon and moderate southerlies during summer offer opposing and aiding effects on sea breeze which can affect the thunderstorm characteristics like development, movement and intensity in the respective seasons. In this work, the impact of sea breeze processes on the development of thunderstorms during the summer (pre-monsoon) and southwest monsoon seasons under different synoptic flow conditions is studied by numerical simulations using WRF. The objective of this study is to analyze the impact of sea breeze circulation on thunderstorm characteristics through various factors such as synoptic flow, moisture transport, convergence, instability, and wind shear. The remainder of the manuscript is organized into five sections. Section 2 gives a description of the study region, Sect. 3 gives description of selected thunderstorms, Sect. 4 gives details of data sets used in the study along with model configuration and numerical simulations. The results of the numerical simulations are provided in Sect. 5 and finally Sect. 6 gives the main conclusions of the study.

2 Study region

In this study, we examine thunderstorms over the southeast coast of India covering an area of 250 × 250 km extending from Nellore in Andhra Pradesh to Karaikal in Tamilnadu (Fig. 1). The region of interest has plain terrain with elevation varying from 6 to 50 m and is surrounded by the Bay of Bengal (BOB) on the eastern side (Revanth Reddy et al. 2020). This region experiences three major synoptic flows (i) southerly flow during the pre-monsoon period (March–May) (ii) south-westerly flow during the summer monsoon (June–September) and north-easterly flow during the winter monsoon (Oct–Dec). The land cover comprises mainly agricultural/croplands, deciduous forests, mixed forests, grasslands, scrublands and urban areas. The soil is sandy-clay and clay across the coast. The study area has two 50-m instrumented micrometeorological towers at Kalpakkam station, Automated Weather Stations (AWS) installed by Indian Space Research Organization (ISRO) at Meenambakkam near Chennai, Vellore, Auroville, Sirugamani, Mailam and Thiruvannamalai and Radiosonde operated by the India Meteorological Department (IMD), Chennai.

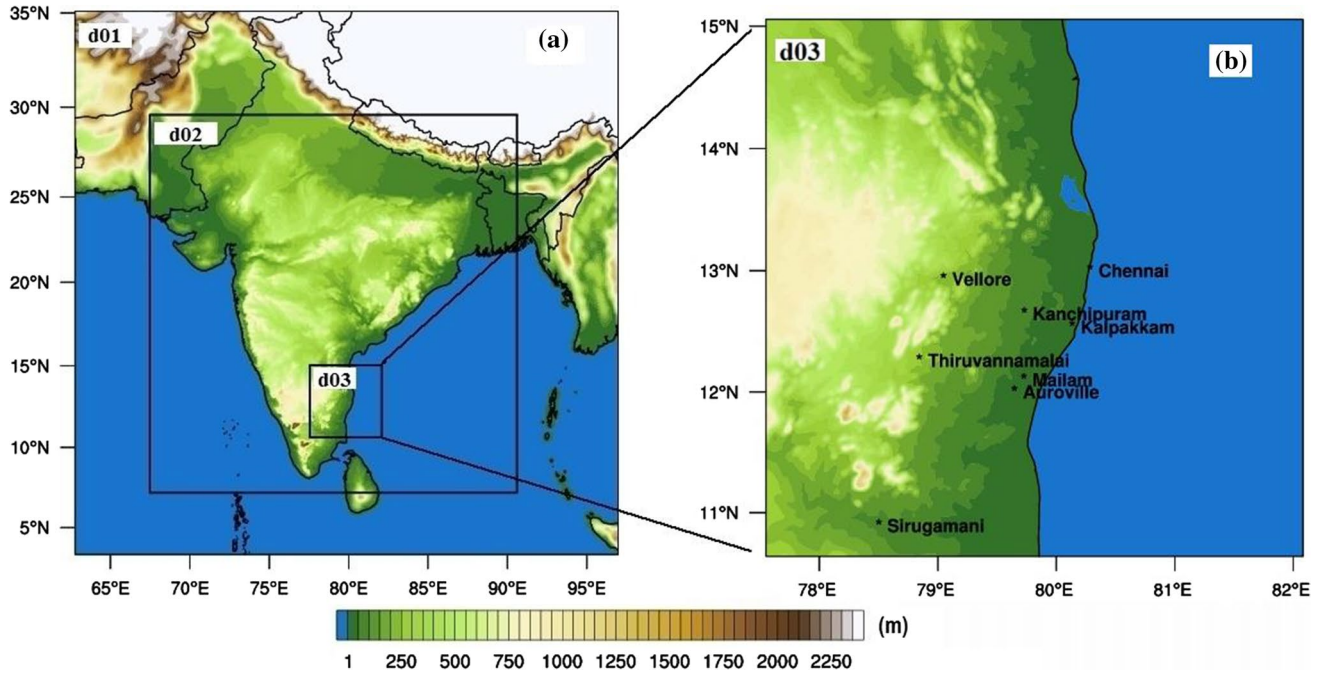

Fig. 1 Simulation domains along with terrain elevation (shaded) **a** Right panel **b** shows the model inner domain with locations of observation stations used for model comparisons

3 Description of thunderstorm events selected for simulations

In this study, two thunderstorm events associated with sea-breeze circulation which occurred in southeast India (i) 24 April 2015 (TS1) during summer and (ii) 22 July 2015 (TS2) during southwest monsoon between Chennai and Karaikal are selected for the study. The event TS1 originated near Vellore (12.9° N; 79.1° E) at 11 UTC/ 17 IST and sustained up to 13 UTC/19 UTC (2 h) on 24 April 2015. The event TS2 originated near Kanchipuram (12.81° N; 79.69° E) at 15 UTC/21 IST and sustained upto 17 UTC/23 IST on 22 July 2015. The large-scale flow was southerly for TS1 and southwesterly for TS2. Though summer and southwest monsoon have nearly similar thermodynamic environment, there are large differences in the characteristics of upper and lower-level circulations in these two seasons (see Sect. 5.1).

4 Data and methodology

4.1 Observational data

The fifth-generation gridded European Centre for Medium-range Weather Forecasts ReAnalysis (ERA5) datasets available at $0.25° \times 0.25°$ resolution (Hersbach and Dee 2016) is used for the analysis of the synoptic scale circulations during the TS events. The synoptic scale circulation during April and July months for the selected thunderstorm cases is analyzed from 10 years of monthly average ERA5 data. The seasonal surface meteorological conditions are analyzed from meteorological tower observations at Kalpakkam station (12.5° N, 80.1° E). Model results for surface air temperature, relative humidity, wind speed, wind direction and rainfall are validated using meteorological tower observations at Kalpakkam, and AWS data at Meenambakkam (12.99° N, 80.17° E), Vellore (12.93° N, 79.02° E), Auroville (12.00° N, 79.81° E), Sirugamani (10.89° N, 78.54° E), Mailam (12.1° N, 79.6° E) and Thiruvannamalai (12.23° N, 79.07° E) sourced from Indian Space Research Organization (ISRO) Meteorological and Oceanographic Satellite Data Archival Centre (MOSDAC) site (http://mosdac.gov.in). Simulated spatial daily rainfall is validated with the multi-satellite-rain gauge merged rainfall data generated by IMD (Mitra et al. 2009). The thermodynamical parameters such as Convective Available Potential Energy (CAPE), Convective Inhibition (CIN) for determining the thunderstorm potential are analyzed from IMD radiosonde vertical profiles at Chennai station. The IMD Doppler Weather Radar (DWR) reflectivity observations are used for evaluation of simulated radar reflectivity and cloud pattern.

4.2 Simulation setup

Numerical simulations of the thunderstorms over the southeast coast were performed using the Advanced Research

Weather Research and Forecasting (WRF-ARW) mesoscale model (version 3.9.1). The model is configured with three nested domains (18, 6, 2 km) (Fig. 1) with 45 vertical levels and the model top is fixed at 50 hPa. The outer domain (d01) covers the Indian sub-continent and the surrounding North Indian Ocean with domain extents of 3.31°–35.09° N latitude and 62.77°–96.96° E longitude; the intermediate domain (d02) covers major land portions of India with domain extents of 7.19°–29.58° N latitude and 67.48°–90.61° E longitude and the high-resolution inner domain (d03) covers the southeast coast from Nellore in Andhra Pradesh to Karaikal in Tamil Nadu with domain extents of 10.63°–15.05° N latitude and 77.55°–82.08° E longitude. The inner domains d02 and d03 are two-way interactive. The land use and land cover, terrain elevation and soil types are defined from the 20 category Moderate Resolution Imaging Spectrometer (MODIS) data, United States Geological Survey (USGS) elevation data and Food and Agriculture Organization (FAO) soil data sets, respectively. All these data available at 5′, 2′ and arc 30 s resolutions are interpolated to the model domains d01, d02 and d03, respectively. The model physics for the simulations is selected based on earlier studies over the southeast coast (Hariprasad et al. 2014; Hari Prasad et al. 2016; Srinivas et al. 2016; Reshmi Mohan et al. 2018 and 2019) and includes Dudhia scheme for short wave radiation (Dudhia 1989), RRTM scheme for long-wave radiation (Mahrer and Pielke 1977), MM5 surface layer similarity scheme for surface layer physics, Noah land surface model (LSM) for the land surface, YSU first order scheme (Hong et al. 2006) for PBL turbulence and Kain-Fritsch (KF-Eta) mass flux scheme for convection (Kain and Fritsch 1993). Convective parameterization was switched off in the inner domain (d03). The Morrison double moment microphysics scheme (Morrison et al. 2009) which includes six hydrometeors (water vapor, cloud droplets, cloud ice, rain, snow and graupel/hail) is used in all the domains based on Halder and Mukhopadhyay (2016).

The model is initialized using the National Centre for Environmental Prediction (NCEP) 1° × 1° resolution Global Forecast System (GFS) Final Analysis (FNL) data and the lateral boundary conditions of the outer domain are updated with the FNL data at every 6 h. The model is initialized at 12 UTC 23 April 2015 for TS1 and 12 UTC 21 July 2015 and in each case the model is integrated for 60 h. The first 12-h of each simulation is considered as spin-up period which is excluded from the analysis. The initialization fields from FNL include the 3D data of temperature, U and V components of wind, relative humidity, geopotential height on constant pressure levels, 2D data of surface pressure, mean sea-level pressure, skin temperature/SST, 2 m temperature, 2 m relative humidity, 10 m U and V components of wind, soil moisture and soil temperature in different ground layers, soil height, water equivalent snow depth, and sea ice.

5 Results and discussion

First, we analyze the low-level atmospheric circulations during the evolution of the Thunderstorms over southern peninsular India using 10 years monthly average ERA5 reanalysis data and thermodynamic environment using available radiosonde data. This will be followed by the analysis of numerical simulations for the two selected thunderstorm cases, their dynamical and thermodynamical features to understand the impact mechanisms of sea-breeze circulation on the thunderstorms in the summer and southwest monsoon periods.

5.1 Environmental setting

The characteristics of low-level circulations, meteorological parameters and thermodynamical indices in summer and southwest monsoon analyzed from various data are presented here. Figure 2 shows the 10-year (2009–2018) mean wind flow analyzed from ERA5 data at the surface [10 m above ground level (agl)] and 925 hPa in the lower atmosphere over southern peninsular India at three synoptic hours (00 UTC, 06 UTC, 12 UTC) for April 2015 during summer and July 2015 during monsoon seasons. As shown in Fig. 2, the period April is characterized by relatively high pressure (1008–1010 hPa) conditions associated with a moderate (2–4 ms^{-1}) southerly flow at 00 UTC (Fig. 2a) and south-southeasterly flow at 06 UTC and 12 UTC (Fig. 2b, c) in the lower troposphere over the east coast. The south-southeasterly winds intruding upto 150–200 km inland along the southeast coast at 06 UTC/12 IST suggest the development of sea-breeze circulation in the daytime. The circulation pattern at 925 hPa level during April (Fig. 2d–f) is similar to the surface flow and the sea breeze can be seen at 12 UTC. The flowfield both at the surface (Fig. 2g–i) and 925 hPa (Fig. 2j–l) during July shows strong westerly/southwesterly winds (~ 5–8 ms^{-1}) suggesting mainly strong monsoon flow over southern peninsular India during July. The calm southerly winds in April (Fig. 2e, f) and strong westerly winds in July indicate weak and strong synoptic forcing during daytime in summer and monsoon, respectively. The weak southerly flow during summer facilitates the development of sea breeze over the southeast coast in summer compared to the opposing strong synoptic flow in the southwest monsoon. Thus, the low-level circulation in summer shows more predominant sea breeze-type mesoscale features compared to monsoon. An interesting feature noted in both summer and monsoon is cold air advection at lower levels to the east coastal parts from highland areas in the western/northwestern parts of the southern peninsula. The

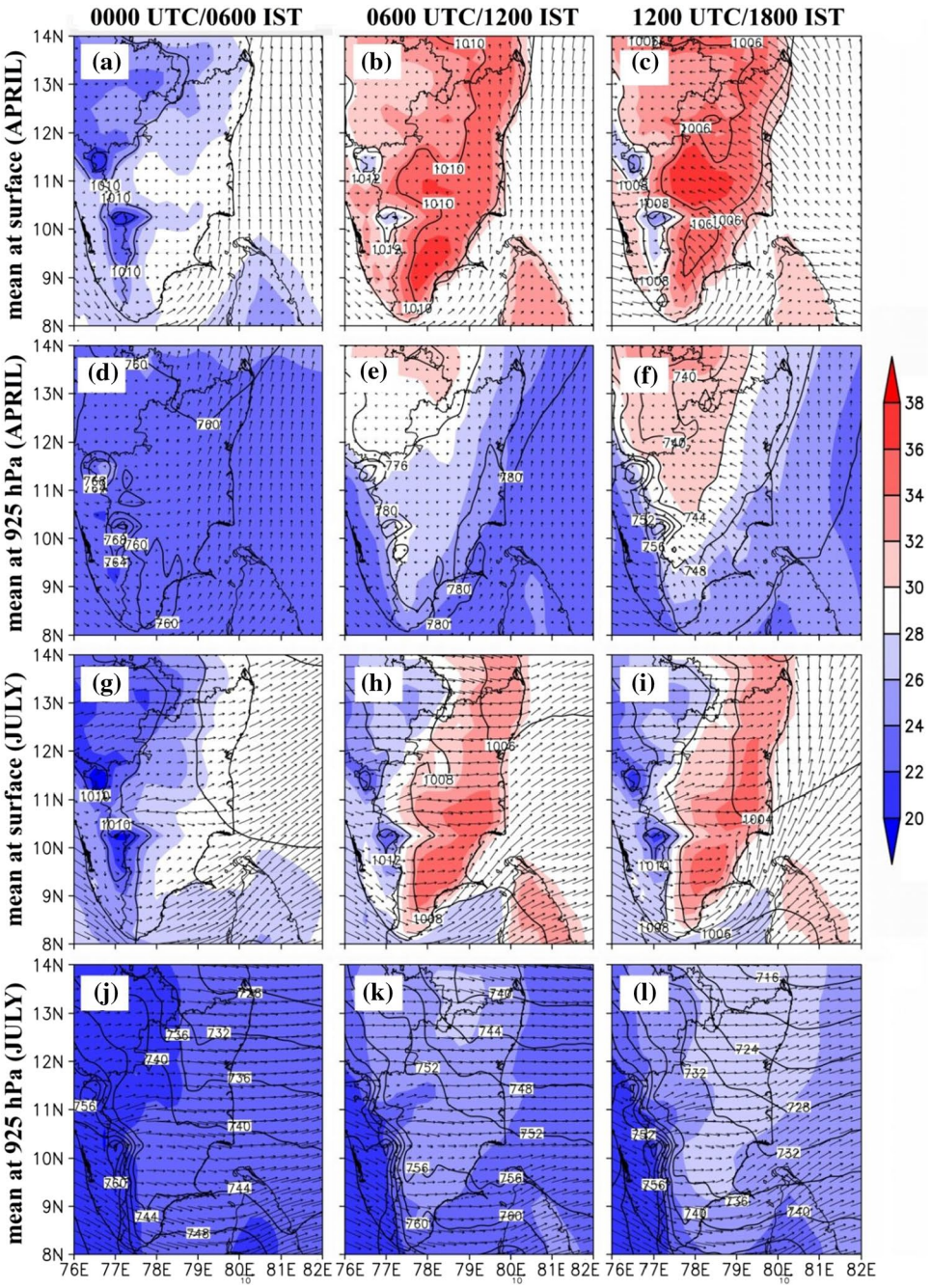

Fig. 2 Comparison of synoptic condition at the surface (SLP, 2 m air temperature & winds) during April (**a**–**c**), July (**g**–**i**) and 925 hPa (Geopotential height, temperature and winds) during April (**d**–**f**), July (**j**–**l**) for 00, 06 and 12 UTC, respectively, from ERA-5 monthly averaged data over 10 years (2009–2018)

time-height section of wind flow (Fig. 3) at Kalpakkam coastal station (12.5° N, 80.10° E) shows diurnally varying wind patterns in the lower levels (below 850 hPa) in both April and July with southeasterly winds between 08 and 18 UTC (14-00 IST) in July and 10–12 UTC (16–18 IST) in monsoon suggesting a longer period of sea breeze in April compared to July. Weak and consistent northeasterly winds in the layer 800–600 hPa (roughly 2–4 km), weak westerly winds in the layer 600–400 hPa (roughly 4–8 km) and easterly winds in the upper troposphere (roughly 8–10 km) are seen in April. The consistent upper level (700 hPa) circulation characterized by a small variation in wind speed (3.0 ms^{-1}) and very small variation in wind direction (3 deg) suggest highly favorable synoptic conditions (Arrillaga et al. 2016) for sea breeze development in summer (Table 1). A high land-sea temperature difference of 3.4 K is also found in ERA5data which satisfies the minimum difference (2.0 K) requirement for sea breeze development. The low-level wind flow during April (Fig. 3a) shows a wind direction shift of 45 deg satisfying the minimum wind shift of > 22.5 deg confirming sea breeze development during 08–18 UTC (14-00 IST) at the

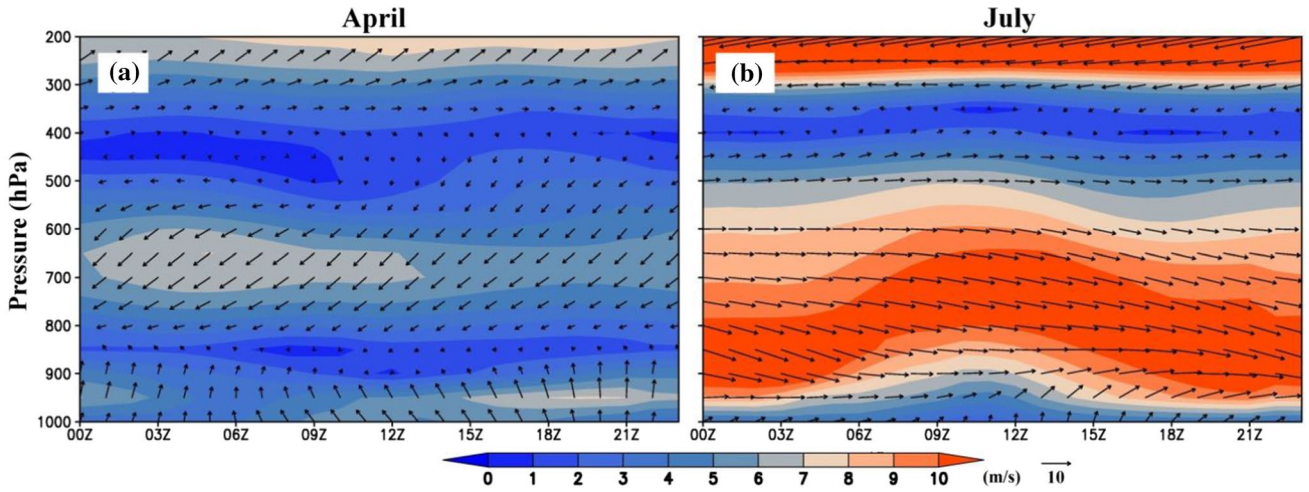

Fig. 3 Time-height section of winds at Kalplakkam station (12.56° N, 80.10° E) from monthly averaged ERA data over 10 years (2009–2018) for **a** April and **b** July

Table 1 Upper air and surface conditions during the sea breeze for the selected thunderstorm cases analyzed from ERA-5 reanalysis data

Parameter	TS1 24-04-2015	TS2 22–07-2015
Wind direction shift at 700 hPa (00 Z) (< 90 deg)	6.5	12.28
Wind speed difference at 700 hPa (00Z- 12Z) (< 6 m/s)	3.01	3
Max wind speed (< 11 m/s)	3.47	8.7
Land sea temperature difference (50 X 50 km) (> 2 °C)	3.4	3.6
Surface wind direction shift (> 22.5 deg)	45.5	106.2
Surface wind direction consistency ratio (> 3)	5.9	13

coastal station Kalpakkam (Revanth Reddy et al. 2022). The time evolution of winds during July (Fig. 3b) shows strong westerly winds (≥ 9 ms^{-1}) in the layer 800–600 hPa throughout the day suggesting uniform monsoon flow and that the sea breeze is mainly confined to the lower levels below 800 hPa and for a limited period (10–12 UTC/16–18 IST). The vertical wind pattern suggests the presence of upper layer wind shear and opposing synoptic conditions for the development of sea breeze over the southeast coast. The differences in the low-level circulations between summer and monsoon synoptic conditions are also seen from the surface wind speed and wind direction data from the meteorological tower at Kalpakkam (Fig. 4). It may be seen that the summer sea breeze has relatively higher intensity (4–6 ms^{-1}) and longer duration (1000–2300 IST) compared to that in monsoon which has less intensity (3–4 ms^{-1}) and shorter duration (1600–2300 IST).

A few thermodynamical indices such as convective available potential energy (CAPE), convective inhibition energy (CIN), total totals index (TTI) and severe weather threat index (SWEAT) associated with convective storms are analyzed from daily radiosonde observations of Chennai city in north coastal Tamilnadu for the period 2015–2019. It has been found that while the TTI and SWEAT are nearly similar in both summer and monsoon (~ 44, ~ 200), the summer has stronger CAPE (1804 J/kg) and lower CIN (– 198 J/kg) compared to the monsoon (CAPE 1213 J/kg; CIN – 91 J/kg). The stability indices for fifteen thunderstorm events that occurred during 2015–2019 are listed in Table 2. It can be seen that the summer storms are associated with stronger CAPE (1389–4666 J/kg) and lower CIN (– 306 to – 4 J/kg) compared to monsoon which has relatively lower CAPE (612–3231 J/kg) and higher CIN (– 207 to – 8 J/kg). Based on the differences in the environmental conditions (background flow, wind shear, sea-land temperature contrast, thermodynamical stability) two thunderstorms that occurred on 24 April 2015 during summer and 22 July 2015 during monsoon are considered for numerical simulations. A detailed analysis of simulations for these two cases is presented below.

5.2 Simulated wind flow field and convergence

The low-level wind flow characteristics during the two thunderstorm events are analyzed to understand the differences in dynamic factors in the two cases. Figure 5 shows

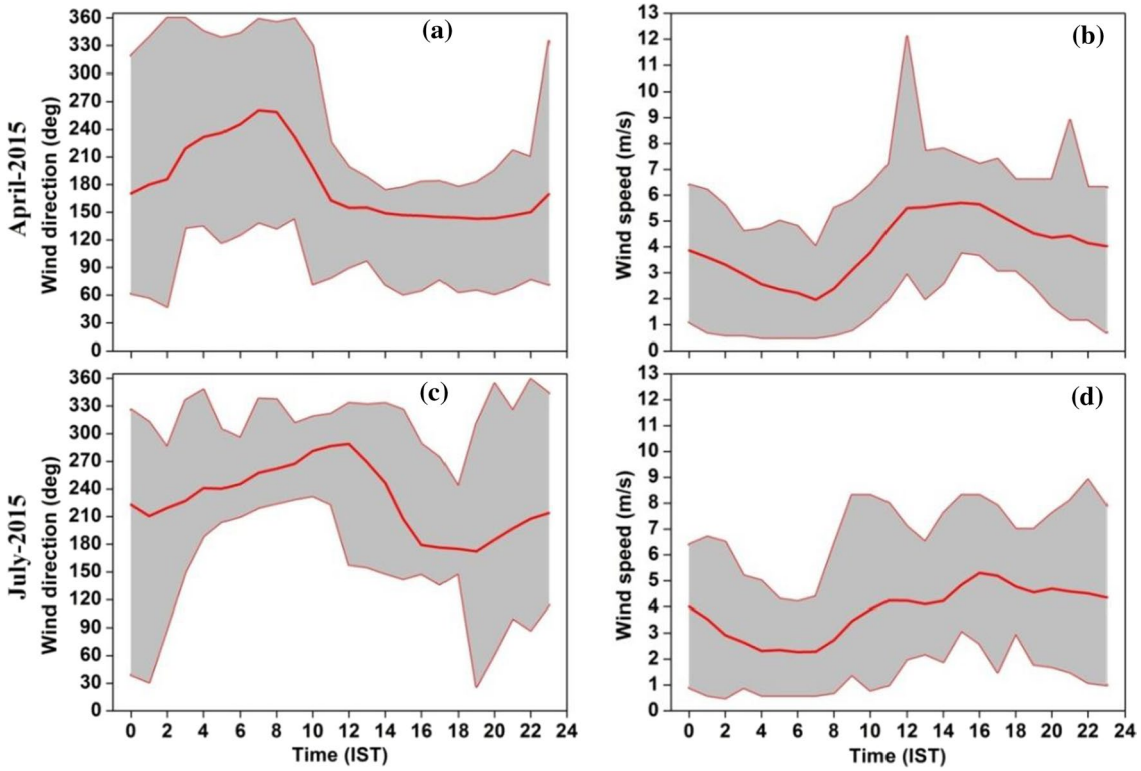

Fig. 4 Time series of surface wind speed and wind direction **a**, **b** for April 2015 **c**, **d** July 2015 from meteorological tower observations at Kalpakkam station (12.56° N, 80.10° E)

the simulated 10 m surface wind field and 2 m air temperature from the model innermost domain at three different instances 10, 11 and 12 UTC on the selected days. Simulations for 24 April (Fig. 5a–c) show weak westerly synoptic flow in the western land areas, and advection of cold air from west central and central hilly areas towards the east coast and development of a cold pool in central parts near Bangalore (13.0° N and 78.5° E). Establishment of land-sea temperature contrast of ~ 5° C and the onset of sea breeze indicated by southerly and south-easterly onshore flow are noticed at 06 UTC/12 IST (not shown). Divergent winds in association with the development of a cold pool in the central parts are seen for TS1. The sea breeze with wind speeds of 6–9 m/s gradually progressed upto ~ 150 km inland by 12 UTC/18 IST (Fig. 5a–c). Simulations also show that the cold pool gradually expanded to the south by 12 UTC/18 IST. The cold pool and sea breeze in the simulation are well separated from each other till 12 UTC/18 IST and they got merged in the northwestern parts of Tamil Nadu at 14 UTC/20 IST (not shown).

For the TS2 event on 22 July 2015 (Fig. 5d–f), we can notice strong westerly synoptic winds (5–6 ms^{-1}) inland, land-sea temperature gradient of ~ 4° C and incidence of south-easterly/easterly winds onshore indicating the onset of the sea breeze at the coast at 10 UTC/ 16 IST. The sea breeze intensity for the monsoon event is relatively weak (4–5 ms^{-1}), progression is not uniform across the coast and the horizontal intrusion is limited to 30–40 km inland. The presence of strong westerly low-level jet (Findlater 1969; Xavier et al. 2017; Viswanadhapalli et al. 2019) (Fig. 5d–f) during monsoon opposes the sea breeze, delays the propagation of sea breeze which leads to the late evening thunderstorms. Similar to summer, the advection of cold air from western hilly areas to the central and eastern parts and intermittent multiple cold pools in southern parts can be seen during the monsoon event but the cold pool areas are less intense during monsoon (Fig. 5d–f). Model simulated wind speed and wind direction on 24 April and 22 July are in good agreement with observations (Fig. 12) at Auroville and Chennai stations suggesting a good simulation of the flowfield.

As the sea breeze progresses inland it transports moist air which by convergence with the synoptic flow forms a front, triggers convection along the sea breeze front which determines the location and intensity of the storm (Shepherd et al. 2001). As shown in Fig. 6, the convergence of the sea breeze with the synoptic flow at several zones in the direction of sea breeze progression is noticed in both the summer and monsoon cases. Simulations show that the sea breeze during the summer case progressed faster, covered nearly 150 km

Table 2 Total observed rainfall (mm) and thermodynamic indices for 15 thunderstorms occurred over the southeast coast of India during the period 2015–2019

S.No	Date (DD-MM-YYYY)	Rainfall (mm) & location	CAPE	CIN	LI	SWEAT	*K*-index	TTI
Summer								
1	24-04-2015	45 (Auroville)	3795.4	−49.1				
2	15-05-2015	31.8 (Kalpakkam) 29.7 (Anupuram)	2371.7	−4.3	−5.93	230.41	37.3	46.3
3	27-05-2015	42 (Sirugamani)	2584.1	−306.3	−6.08	305.01	38.5	52
4	17-03-2018	35.5 (Kalpakkam) 31.4 (Anupuram)	1389.3	−3.53	−0.3 −2.84	216.59 153.40	34.2 29.5	44.4 39.6
5	22-04-2019	24 (Kanchipuram)	2166.3	−104.9	−7.17 −5.57	264.41 178.2	36.5 30.3	51.6 44.4
6	07-05-2019	Kanchipuram IMD DWR	4666.5	−64.6	−2.55 −8.03	154.39 334.99	29.1 34.4	40.8 51.8
7	08-05-2019	Kanchipuram IMD DWR	1646.1	−215.8	−1.6 −3.77	175.81 232.81	35.7 36.9	46.6 49.0
SWM								
8	22-07-2015	25.6 (Kalpakkam) 29.4 (Anupuram)	612.5	−172.87	−2.16	224.19	33.3	45.4
9	06-06-2017	10.0 (Anupuram)	703.8	−207.09	−2.4 −2.14	235.22 248.58	39.9 40.9	46.8 47.6
10	02-06-2018	Chennai IMD DWR	2031.9	−120.23	−2.25 −4.86	230.01 229.2	37.4 34.1	45.5 48
11	26-06-2018	Chennai IMD DWR	1579.6	−129.19	−0.71 −3.6	220.59 238.42	36.4 42.0	44.0 48.0
12	02-07-2018	Chennai IMD DWR	2031.9	−120.23	−2.47 −3.46	221.59 231.38	37.7 38.1	46.9 46.0
13	26-06-2019	26.5 (Kalpakkam) 27.5 (Anupuram)	3231.4	−7.81	−4.44 −5.18	241.41 231.99	38.9 37.0	46.0 48.0
14	25-07-2019	7.0 (Kalpakkam) 35.1 (Anupuram)	2527.9	−29.78	−1.92 −5.56	233.8 245.01	37.7 37.8	46.4 46.0
15	18-08-2019	29.5 (Anupuram)	726.1	−126.8	−3.62 −1.82	224.20 220.98	40.3 35.4	48.4 43.4

across the coast (Fig. 6a–c) whereas during the monsoon case it progressed slowly due to opposing large-scale winds and intruded over 40 km across the coast by 12 UTC /18 IST (Fig. 6b–d). Simulated flow convergence pattern for 24 April indicates that the sea breeze front aligned parallel to the coast is located at about 79.7 Eat 10 UTC/16 IST and gradually moved further inland to 79.0 E at 12 UTC/18 IST. A circular flow convergence is also seen along the boundaries of the cold pool in central parts of the domain which gradually moved to the south-eastern parts. The convergence along the sea breeze front leads to instability and provides the necessary mechanism for convection and storm development (Simpson et al. 2007). The convergence zones of the cold pool and sea breeze got merged in the evening by 12 UTC/18 IST. DWR reflectivity images for TS1 suggest convective cloud development along the areas of flow convergence on 24 April. DWR data shows that clouds started developing at 10 UTC/16 IST 24 April (Fig. 7a) at (i) sea breeze frontal zone (12.5° N, 79.5° E) near the coast and (ii) near the cold pool in central areas (13.0° N, 78.5° E) indicating genesis of separate convective storms at these two locations. The areas of clouds gradually enhanced at both the above locations during 10–12 UTC/16–180 IST 24 April (Fig. 7a–c) until both the storms got merged at around 14 UTC/20 IST. This suggests that the thunderstorm near the coast was initiated by flow convergence and convection at the sea breeze front rather than due to the cold pool effect ahead of the sea breeze front. However, the more intensified storm at 14 UTC/20 IST (Fig. 7d) is possibly due to the cold pool as the latter can initiate secondary convection and lead to the development of deep convection by injection of moisture into the boundary layer from the precipitating downdrafts (Schlemmer and Hohenegger 2014; Marion and Trapp 2019). The presence of the sea breeze convergence zone and cold pool is clearly represented in the IMD DWR reflectivity images at 11 and 12 UTC (Fig. 8e–h). The simulated hydrometeor reflectivity pattern (Fig. 7e–h) shows the individual cloud bands in association with the storms developed at the cold pool and

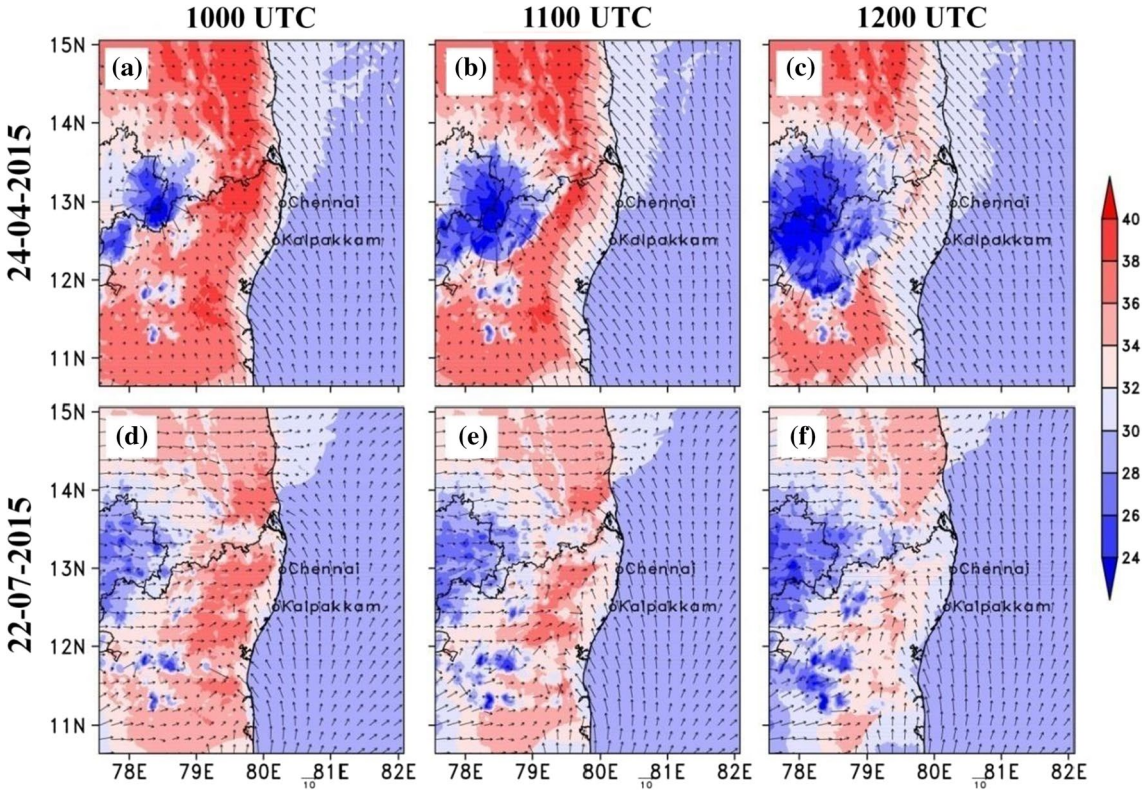

Fig. 5 Simulated surface wind flow at 10 m and air temperature at 2 m (shaded). Top panels (**a**–**c**) are at 10 UTC/16 IST, 11 UTC/17 IST and 12 UTC/18 IST on 24 April 2015 for TS1 and bottom panels (**d**–**f**) are at 10 UTC/ 16 IST, 11 UTC/17 IST and 12 UTC/18 IST on 22 July 2015 for TS2

sea breeze front zones and their subsequent merging at 14 UTC/20 IST similar to the features in DWR data, but with stronger intensity.

Convergence of sea breeze with large-scale winds can be seen at multiple zones for TS2 (Fig. 6d–f), however, it is less organized and less intense compared to the summer case TS1. The convergence is stronger ($180–280 \times 10^{-5}$/s) and aligned parallel to the coast between 12° and 14° N for the summer case TS1 (Fig. 6a–c) whereas it is relatively weaker ($120–180 \times 10^{-5}$/s) with wavy pattern aligned along an intermittent sea breeze front between 11.5° and – 13.5° N for the monsoon case TS2 (Fig. 6d–f). Simulated convergence patterns suggest the development of a stronger front in TS1 compared to TS2. We have analyzed the time series of flow convergence over an area of 0.5×0.5 deg at the originating location of the sea breeze front i.e., 12.0° N and 79.5° E for TS1 and 12.9° N and 80.1° E for TS2 (not shown). It is noticed that convergence is about 3 times stronger (9.0×10^{-5} /s) in TS1 compared to TS2 ($3.0 \times 1.e–^{5}$/s). DWR data for TS2 shows two cloud bands on 22 July at (i) sea breeze frontal zone (12.75° N, 79.5° E) in north coastal Tamil Nadu and (ii) near the cold pool areas in interior southern Tamil Nadu (11.8° N, 78.8° E). This suggests the development of separate convective storms at the above locations. The DWR data indicates a gradual southward movement of cloud bands associated with a sea breeze storm and a northeastward movement of cloud bands from southern cold pool areas during 10–12 UTC/16–180 IST 22 July (Fig. 7i–l) until both the cloud bands got merged at around 12 UTC/18 IST. However, the simulation for TS2 poorly represented the cloud pattern in comparison to DWR observed reflectivity at the corresponding times and this discrepancy is mainly due to the model storm developing slightly late by 2 h compared to the actual storm. Simulated hydrometeor reflectivity (Fig. 7m–p) indicates the model storm is less intensive compared to the observed storm for the monsoon case.

Figure 8 shows the longitudinal height section of horizontal winds (vectors), water vapor mixing ratio and vertical motion (shaded) across the east coast for the two TS cases. We notice strong vertical motions extending from the surface to the upper troposphere in the sea breeze frontal zone between 10–12 UTC/16–18 IST and above 800 hPa (~2 km) near the cold pool over central hilly areas at 11 UTC/17 UTC and represent convective motions associated with the thunderstorms at respective locations. The cores of vertical motion are surrounded by downdrafts on either side of both the convective cells. As evident from a vertical section at 11 UTC/17 IST (Fig. 8b) the convection near the cold pool

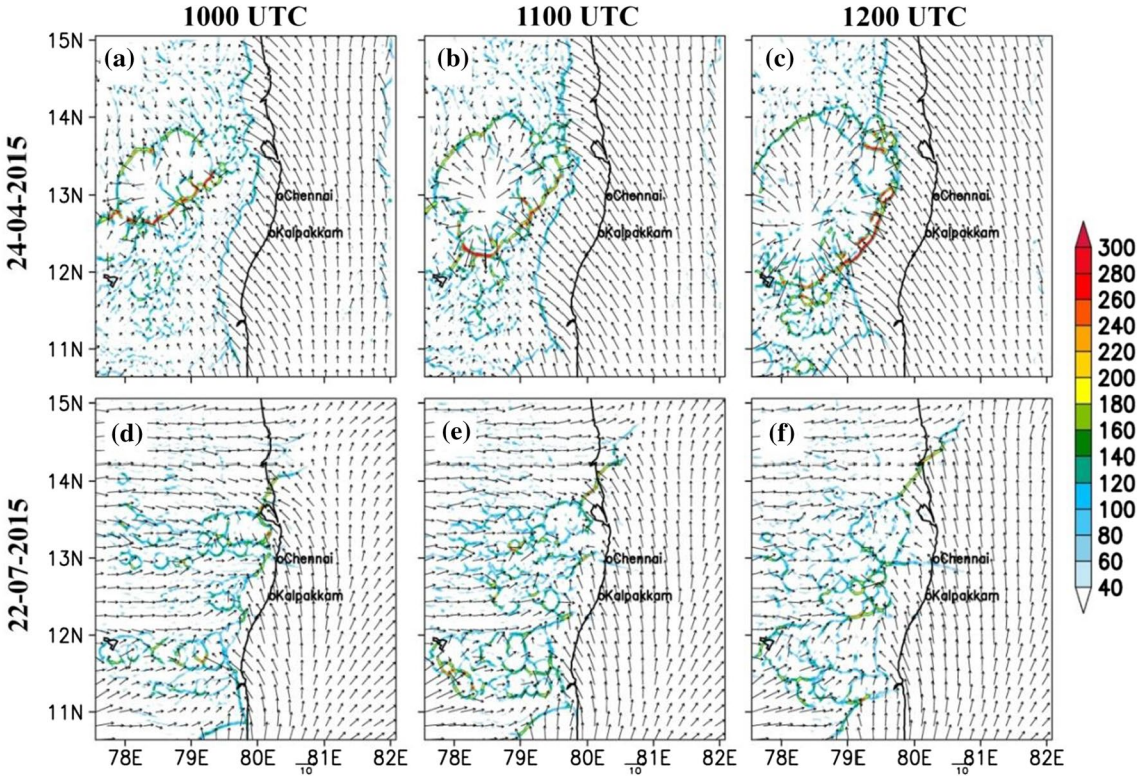

Fig. 6 Simulated surface wind flow field along with convergence (10^{-5}/s). Top panels (**a**–**c**) are at 10 UTC/16 IST, 11 UTC/17 IST and 12 UTC/18 IST on 24 April 2015 for TS1 and bottom panels (**d**–**f**) are at 10 UTC/ 16 IST, 11 UTC/17 IST and 12 UTC/18 IST on 22 July 2015 for TS2

location (77.8° E) is well separated from the convective cell at the sea breeze front (79.2° E) suggesting that the thunderstorm near the coast developed independently from the cold pool inland and that the origin of convection is convergence at sea breeze. This is clearly evident from the flow convergence at lower levels (below 900 hPa) and high vapor mixing ratio (10–12 g/kg) in the frontal convergence zone due to the moisture bought by the sea breeze (Fig. 8a–c). Compared to the summer storm TS1, the vertical motions during the monsoon storm event are less strong and extend to relatively shallow layers in the troposphere in TS2 (Fig. 8d–f).

The sea breeze convergence with the synoptic flow in the boundary layer triggers moist convection. The moisture flux convergence (MFC) along the sea breeze front is computed as integrated horizontal moisture flux convergence between the surface and 300 hPa following (Zhao et al. 2020). The moisture flux is computed from the zonal and meridional components of column-integrated moisture flux between the surface and upper troposphere (300 hPa). The MFC at 15 UTC/21 IST on 24 April 2015 for TS1 is shown in Fig. 9a and at 13 UTC/21 IST on 22 July 2015 for TS2 is shown in Fig. 9b. The moisture convergence along the sea breeze frontal region will lead to moist convection, generation of clouds and precipitation. Moisture convergence in TS1 is relatively stronger and well organized due to more intense sea breeze during the summer season compared to that in the southwest monsoon case (TS2) (Fig. 9b). It can be seen that the moisture convergence for the TS2 (22 July 2015) (Fig. 9b) is not well organized under relatively weak sea breeze compared to the summer event. The week moisture convergence at the sea breeze front during monsoon leads to less vertical moisture transport and thus less intensive thunderstorm compared to the summer case (Poljak et al. 2014).

The differences in vertical moisture transport and convection in the two storm events are analyzed from time-height section of relative humidity and vertical velocity (Fig. 10) around the storm locations. It can be seen that for TS1, the relative humidity starts building up from 09 UTC/15 IST, gradually extends vertically over 10–13 km by 15 UTC/21 IST and continues till 18 UTC/00 IST (Fig. 10a). The maximum humidity (100%) build-up occurs at 15 UTC/ 21 IST over a deep vertical layer associated with high vertical velocity (3 m/s) coinciding with the beginning of rainfall event (Fig. 12e). Similarly, for TS2, the humidity starts building up from 12 UTC/18 IST and reaches a peak (100%) between 15 and 17 UTC/ 21–23 IST with vertical velocity (0.4 m/s) (Fig. 10b) which coincides with the beginning of rainfall (see Sect. 5.3).

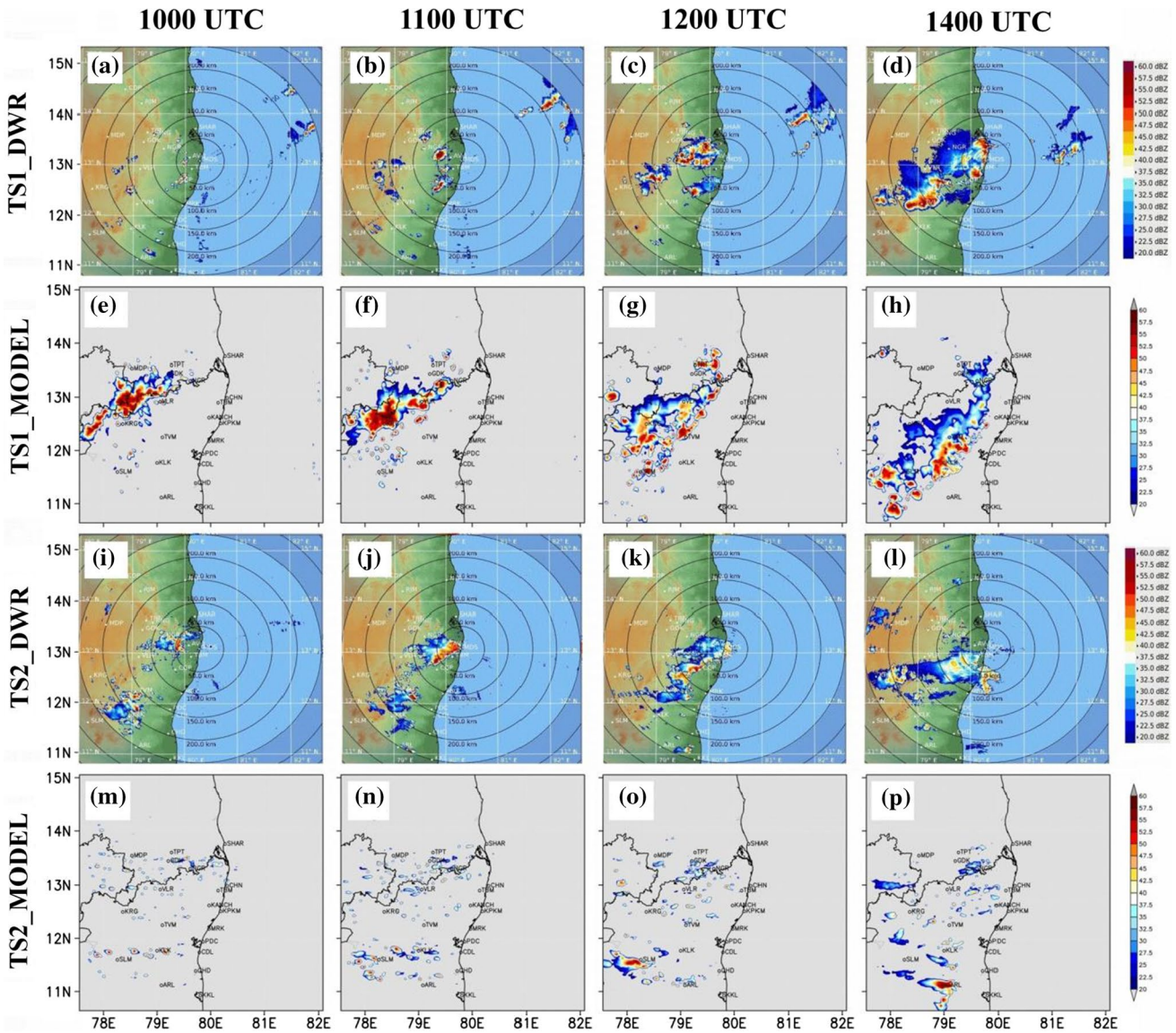

Fig. 7 Observed and model simulated reflectivity (dBZ). First-row panels (**a**–**d**) are observed reflectivity for TS1, second-row (**e**–**h**) are model simulated reflectivity for TS1, third-row panels (**i**–**l**) are observed reflectivity for TS2 and fourth-row panels (**m**–**p**) are model simulated reflectivity for TS2 at 10 UTC/16IST, 11 UTC/ 17 IST, 12 UTC/ 18 IST and 14 UTC/ 20 IST, respectively

A comparison of these vertical sections with the moisture convergence (Fig. 9) suggests that the build-up of humidity occurs in association with the peak moisture convergence at 12 UTC for TS1 and 15 UTC for TS2. The moisture convergence at the lower levels and the presence of mid-tropospheric moisture determines the intensity of convection development by releasing the latent heat (Shepherd et al. 2001). The increase in humidity is also seen to coincide with the increase of theta-e i.e., build-up of instability from 09 UTC/15 IST for TS1 and 15 UTC/21 IST for TS2 (see Sect. 5.4). The intense convergence at lower levels between 79.5° and 79.75° E longitude in TS1 leads to strong vertical transport of moisture to the higher levels during summer case TS1 compared to monsoon case TS2. The increase of humidity from the surface to the mid-troposphere leads to relatively stronger instability compared to TS2. Simulations indicate a stronger sea breeze circulation, stronger convergence and convection (up to 6–7 km) in TS1 compared to TS2 (Table 3). These results suggest that the sea breeze characteristics such as intensity, interaction with the synoptic flow, convergence and vertical moisture transport are slightly different in summer and monsoon cases and play a crucial role in the development of thunderstorms in the two seasons.

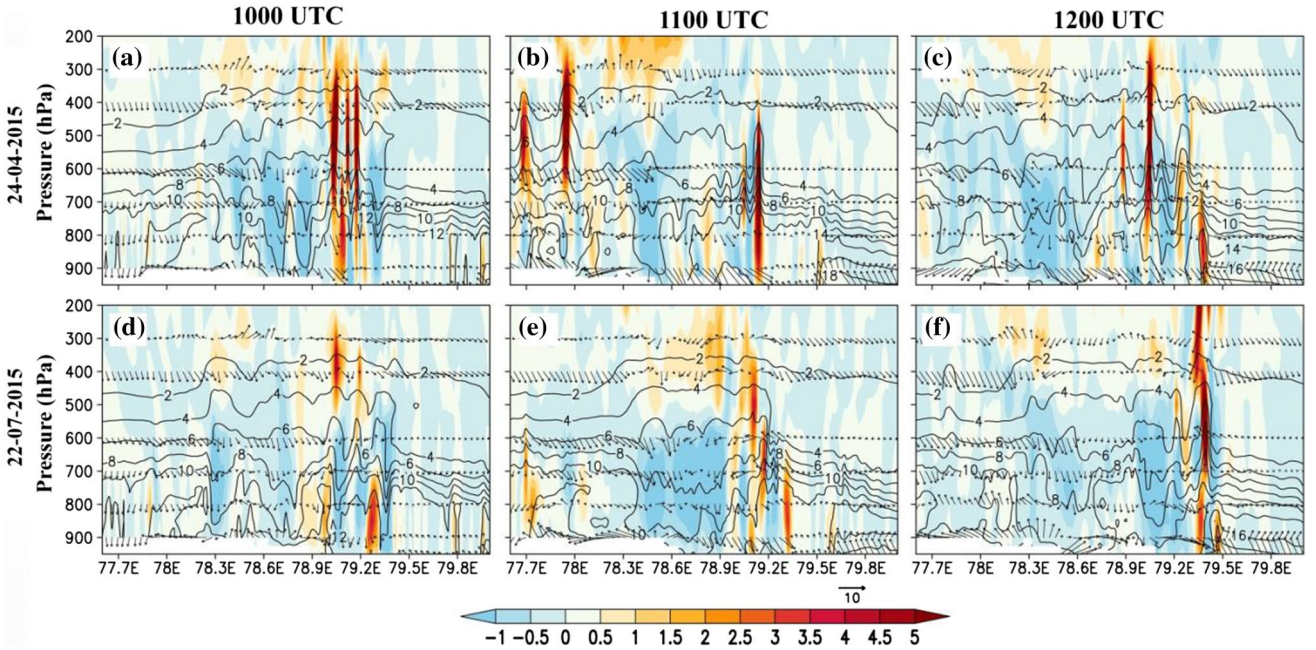

Fig. 8 Simulated longitudinal-height section of vertical velocity (shaded), water vapour mixing ratio (contours).Top panels (**a**–**c**) are at 10 UTC/16 IST (at 13.1° N), 11 UTC/17 IST (at 12.7° N) and 12 UTC/18 IST (at 12.5° N) on 24 April 2015 for TS1 and bottom panels (**d**–**f**) are at 10 UTC/ 16 IST (at 13.2° N), 11 UTC/17 IST (at 12.9° N) and 12 UTC/18 IST (at 12.7° N) on 22 July 2015 for TS2

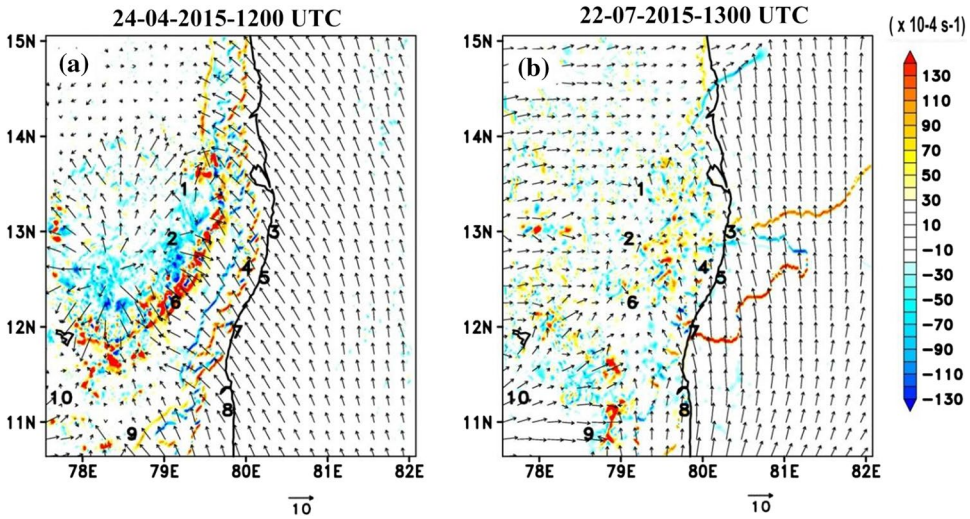

Fig. 9 Simulated surface wind flow (at 10 m) and vertically integrated moisture convergence in the layer 1000–300 hPa at **a** 12 UTC/18 IST on 24 April 2015 for TS1 and **b** 13 UTC/19 IST on 22 July 2015 for TS2

5.3 Simulated rainfall distribution

Simulated 24-h rainfall pattern along with IMD gridded rainfall data for the two thunderstorm cases is presented in Fig. 11. Both observations and simulations show that TS1 (Fig. 11a, b) produced more amount of rainfall spread over a larger area compared to TS2 (Fig. 11c, d), indicating TS1 was a stronger thunderstorm compared to TS2. For TS1, the IMD gridded rainfall data shows two peaks, the first peak (> 70 mm) in the southern end of the domain near Sirugamani and the second peak (> 50 mm) about 75 km southwest of Pondicherry. The gridded rainfall pattern is smooth due to spatial interpolation unlike model-predicted rainfall which shows spatial heterogeneity with peak rainfall located in northwest, coastal Tamilnadu near Pondicherry, and southern parts near Sirugamani and south of Erode. Simulations slightly underestimated the rainfall compared to the gridded rainfall. Time series of simulated rainfall at the Auroville location (Fig. 12c) shows the timing of peak simulated rainfall is a little earlier and the magnitude is slightly less than the rain gauge data, which is because of the difference in the simulated spatial distribution of rainfall.

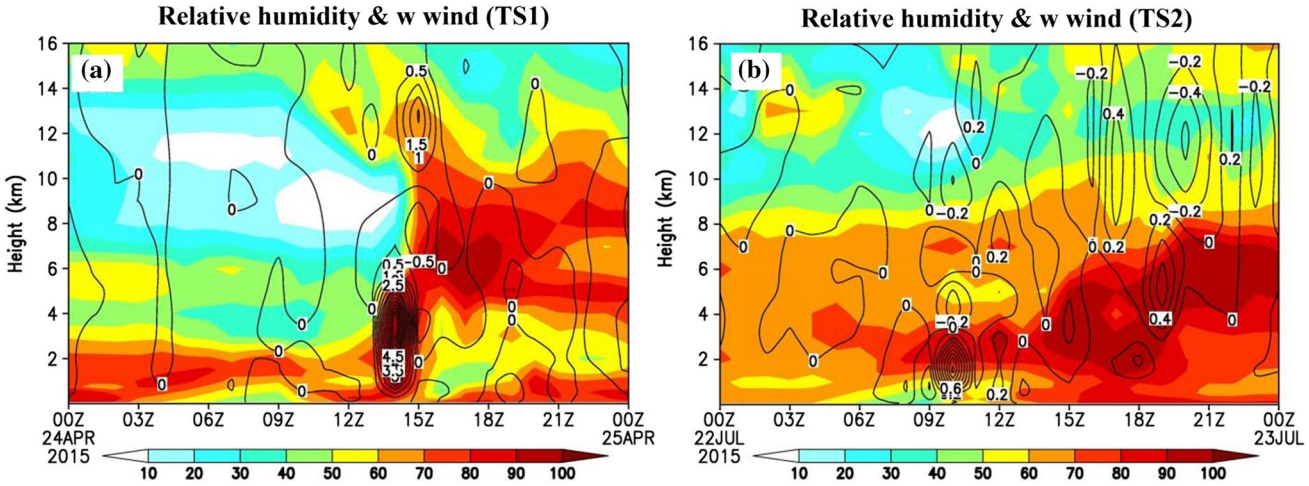

Fig. 10 Time height section of simulated relative humidity (shaded) and vertical velocity (contours) at **a** Auroville for TS1 and **b** Chennai TS2

Table 3 Comparison of simulated meteorological parameters with observations from different thunderstorm cases TS1 on 24 April 2015 at Auroville and TS2 on 22 July 2015 at Kalpakkam

Parameter	TS1 24-04-2015		TS2 22-07-2015	
	OBS	Model	OBS	Model
Total Rain (mm)	45	40.9	26	28.2
Rain onset (UTC)	15	13	13	13
Time of peak rain (UTC)	16	14	13	18
Temperature drop (C) and time (UTC)	30–25 (16)	30–28 (15)	27–23 (14)	28–26 (18)
Increase in Rh (%) and Time (UTC)	67–74 (12)	66–73 (15)	80–94 (14)	78–94 (18)
Sea breeze intensity (m/s)	3.7	7.9	6.1	3.5
Max CAPE (J/kg) (Chennai)	–	3795.36	612.56	562.3
CIN (J/kg)	–	49.1	172.87	103.85
Low-level (surface-700 hPa) Shear (m/s)	–	17.5	–	15
Upper air shear (500 hPa- 200 Hpa) (m/s)	–	18.0	–	40.12
Divergene/ Convergence ($\times 10^{-5}$ /sec)	–	11.2	–	7.2
Vertical motion along sea breeze front (cm/s)	–	28	–	12
Theta-e (k)	–	354.2	–	352.5
Maximum warming (C)	–	12	–	10

The observed rainfall for case TS2 on 22 July 2015 shows the occurrence of about 20–60 mm rainfall distributed from Chennai to Thiruvannamalai and extending further to the west (Fig. 11b, d) with peak rainfall located between Thiruvannamalai and Chengalpattu. Model could reproduce the spatial rainfall pattern for TS2. Comparison with rain gauge data at Meenambakkam (Chennai) station shows that the model reproduced the time of the thunderstorm well but slightly underpredicted the rainfall amount.

The evolution of surface meteorological variables during the storms are analyzed at Auroville for TS1 and Meenambakkam for TS2. As shown in Fig. 12, the storm events are associated with a sudden drop in temperature, increase in relative humidity (RH), increase in wind speed and change in wind direction at the two stations. For TS1, both observations and simulations indicate a sudden drop in air temperature (37–23 °C), rise in RH (50–90%) and an increase in wind speed (3–6 ms^{-1}) at 12 UTC 24 April 2015 at Auroville station. The winds at this station changed to westerly winds around 15 UTC/21IST and simultaneously the temperature is further reduced from 30 to 22 °C and relative humidity increased from 65 to 90% indicating the arrival of the thunderstorm at the station. The abrupt variation in various surface meteorological variables during thunderstorm events is due to large convective updrafts and the mixing of cool air by the

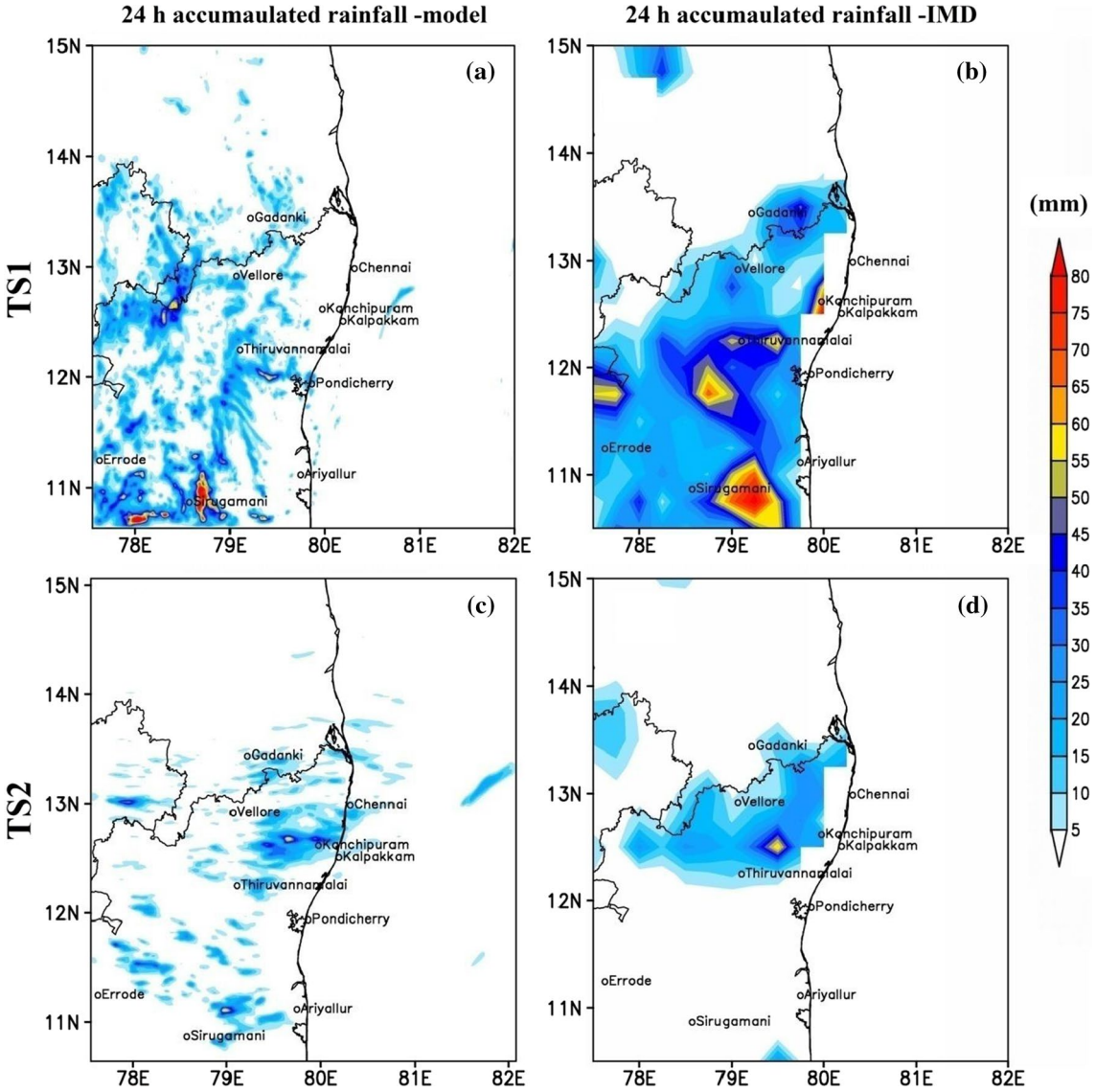

Fig. 11 Comparison of model simulated 24 h accumulated rainfall with IMD gridded rainfall on different thunderstorm days. Top panels (**a**, **b**) are for 24 April 2015 (TS1) and bottom panels are for 22 July 2015 (TS2)

downdrafts (Asnani 2005). Observations show the occurrence of rainfall between 12 UTC/18 IST and 15 UTC/21 IST (Fig. 12c) for TS1(Table 3). For the event TS2 (22 July 2015), observations at Meenambakkam (Fig. 12d–f) indicate an abrupt fall in temperature along with a decrease in wind speed at 12 UTC/ 18 IST and this is associated with rainfall. The model could capture the changes in various parameters along with timing in both the cases (Table 3). However, it has underestimated the RH by 7%, overestimated the temperature by 2.7 °C and wind speed by 1.8 ms^{-1} (Table 4). The large bias of 15.3 deg in simulations is possibly due to not capturing the eddy motions during the storm period. The low humidity in simulations may be due to an increase in horizontal moisture transport by simulating stronger winds. The model underpredicted the rainfall and also shows a slight delay in the onset of rainfall.

5.4 Thermodynamical parameters

The variation in boundary layer characteristics in the two thunderstorm cases is analyzed from the time series of area average sensible heat, latent heat and buoyancy flux (Fig. 13) over a 0.5° × 0.5°region around TS1 at (12.0° N, 79.5° E) and around TS2at (12.9° N, 80.1° E). The buoyancy flux is calculated from the surface sensible and latent heat fluxes (Garratt 1994). Simulated sensible heat flux in TS1 is larger by ~ 100–250 Wm^{-2} and latent heat flux is lower by ~ 300

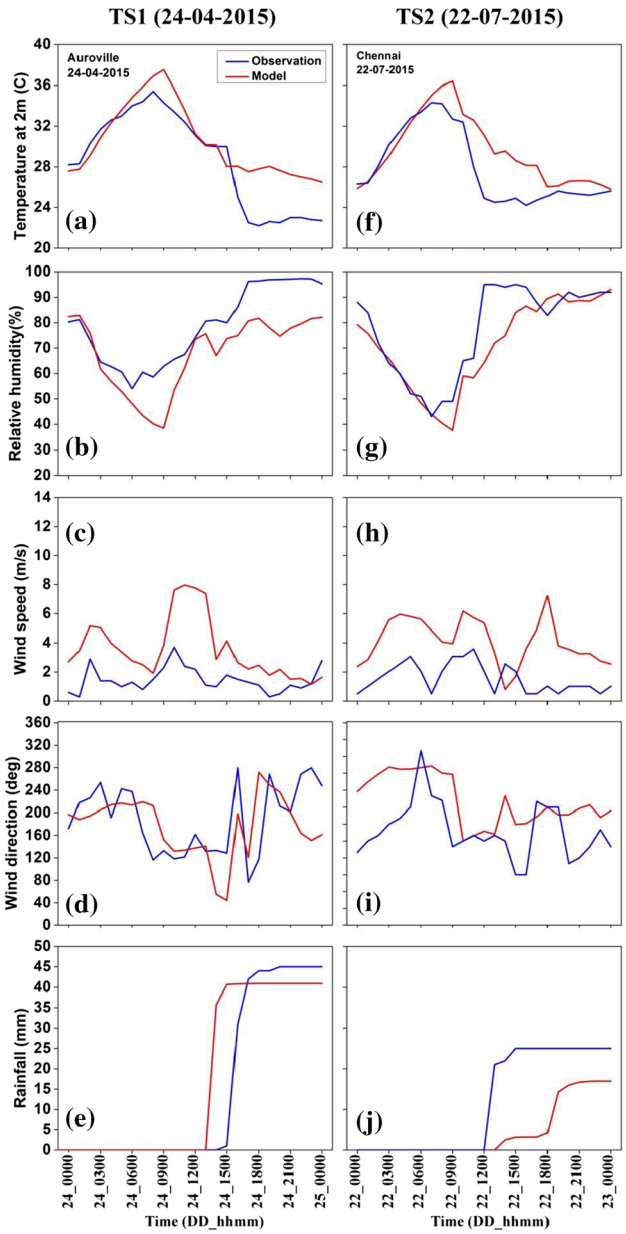

Fig. 12 Comparison of time series of simulated surface meteorological variables (2 m air temperature, 2 m relative humidity, 10 wind speed, 10 m wind direction and rainfall) with AWS observations. Left panels (**a**–**e**) are for TS1 at Auroville AWS station and right panels (**f**–**i**) are for TS2 at Chennai

Wm^{-2} compared to TS2 (Fig. 13a, b) which resulted in a larger buoyancy flux in the summer case. After the storm, a drop in the surface energy fluxes is noticed. The variation in the simulated fluxes of sensible heat and buoyancy between the two seasons in the study region are due to the variation in soil moisture, vegetation and resulting differences in energy partitioning (Rajeswari et al. 2020). The relatively large buoyancy flux during the pre-storm phase in TS1 compared

Table 4 Model error statistics calculated using observations at six surface stations (Auroville, Chennai, Kalpakkam, Thiruvannamalai, Mailam and Vellore)

Parameter	MB	MAE	RMSE	Correlation
Temperature (°C)	2.70	2.98	3.67	0.83
Relative humidity (%)	– 8.2	7.8	9.8	0.9
Wind speed (m/s)	0.87	1.8	2.2	0.6
Wind direction (deg)	15.3	32.3	45.1	0.5
Rainfall (mm)	– 0.24	5.22	10.26	0.75

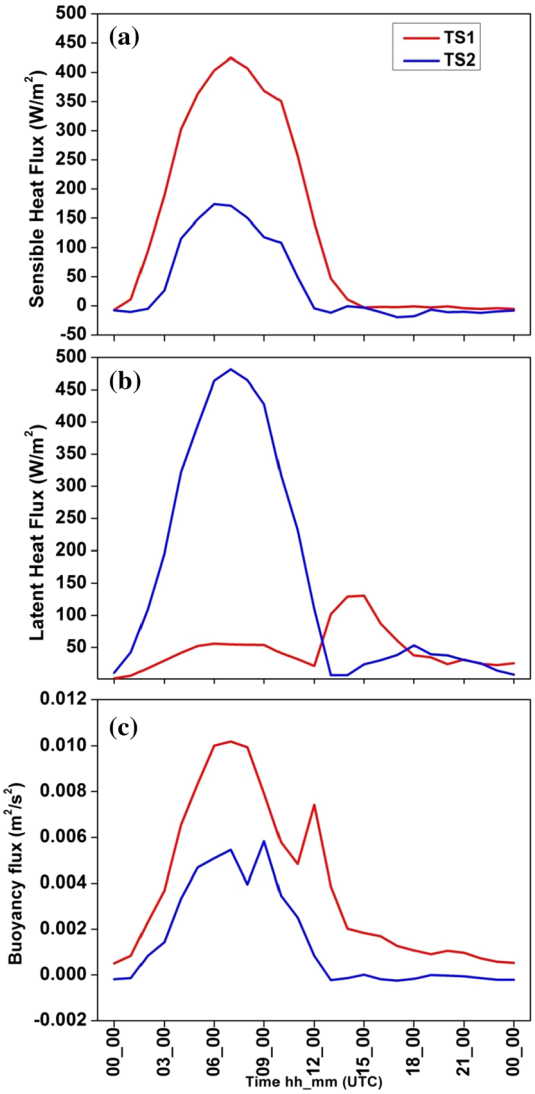

Fig. 13 Time series of simulated area average (0.1 × 0.1 deg) **a** sensible heat flux, **b** latent heat flux and **c** buoyancy flux for thunderstorm TS1 at Auroville and TS2 at Chennai stations

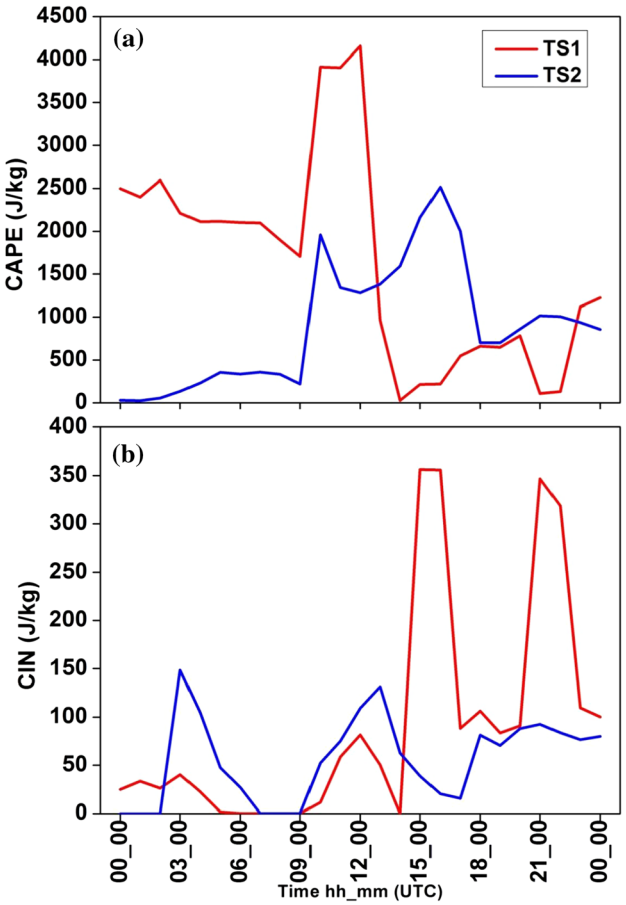

Fig. 14 Time series of simulated area average (0.1×0.1 deg) **a** CAPE and **b** CIN for the two thunderstorm cases TS1 in red at Auroville and TS2 in blue at Chennai

to TS2 promotes stronger free convection in the boundary layer in summer compared to monsoon (Fig. 13c).

The convective environment during the storm events is analyzed from time series of area average CAPE and CIN over a 0.1°×0.1° region near Auroville for TS1 and near Chennai station for TS2 (Fig. 14). An increase of CAPE (Fig. 14a) from a low background value of 1000–3800 J/Kg and decrease of CIN (Fig. 14b) from a high value of 150 J/Kg to the lowest value of 10 J/Kg is noticed by 09UTC/15IST. Subsequently, the CAPE reduced and CIN increased and reached normal values by 18 UTC/24IST. Considering the CAPE and CIN as a measure of convective instability of the atmosphere (Chappell and Smith 1975; Chaudhuri and Bhowmick 2006), the high CAPE and low CIN at 09 UTC/15 IST indicate the development of large instability of the atmosphere for TS1. For the event TS2, CAPE increased from a low background value of 20–2500 J/Kg and CIN decreased from a high value of 150 J/Kg to the lowest value of 50 J/Kg by 15 UTC/21 IST. Subsequently, the CAPE was reduced and CIN was restored to normal values by 15 UTC/21IST for TS3. The time evolution of CAPE and CIN are consistent with changes in surface weather parameters and rainfall associated with the storms (Fig. 14). The stronger convergence and larger moist convection in summer compared to monsoon (Fig. 8, Table 3) led to higher CAPE and lower CIN representing more instability compared to the monsoon storm. The higher CAPE and stronger convection in summer would ultimately influence the raindrop size and precipitation mechanism (Chaudhuri and Bhowmick 2006).

The broad variation in the vertical structure of the two storm events is analyzed from area-averaged vertical profiles of convergence, theta-e, warming and vertical velocity (Fig. 15) over a 0.5×0.5 deg area around the centre of each storm at their peak stage. The warming is computed as the difference in temperature at the mature stage of the storm and the initial stage. Convergence with vertical motion below 3 km and divergence in the middle and upper levels are noticed (Fig. 15). The strong vertical motions/updrafts in both the TS events are associated with strong-low level convergence, and peak phase of the CAPE. A stronger convergence in the lower levels and stronger divergence in the upper levels is noticed in TS1 (Fig. 15a) compared to TS2 (Fig. 15b). It may be seen from a vertical variation of theta-e that the summer event is characterized by relatively more strongly unstable conditions in the lower and middle troposphere (Fig. 15b). The summer event has a stronger vertical velocity (0.04–0.08 m/s) in different layers of troposphere compared to monsoon case (0.01–0.02 m/s) (Fig. 15d) and this is probably due to stronger convergence in TS1. As shown in Fig. 15c we observe warming in the layer 3–10 km in both cases which is due to the diabetic heating by phase changes of moisture. A strong warming in the lower 1–2 km region in the lower atmosphere is noticed. This is possibly due to the combined effects of warm air subsidence due to the downdrafts and evaporative cooling of convective updrafts. Simulations show that the summer event has at least 2–3 °C higher warming compared to the monsoon case. The warming in the middle to upper layers indicates high conditional instability and correlates well with the theta-e, large CAPE and strong vertical motions. The summer event TS1 shows stronger warming in response to stronger convergence, vertical motion, large moisture build-up and high theta-e compared to monsoon case TS2.

5.5 Wind shear

Wind shear plays a major role in the development and movement of thunderstorms. It tilts the storm and separates the updraft and downdraft regions which enhances the storm intensity to sustain for a longer time. The strong vertical shear due to the horizontal winds in the lower levels leads to the production of kinetic energy which leads

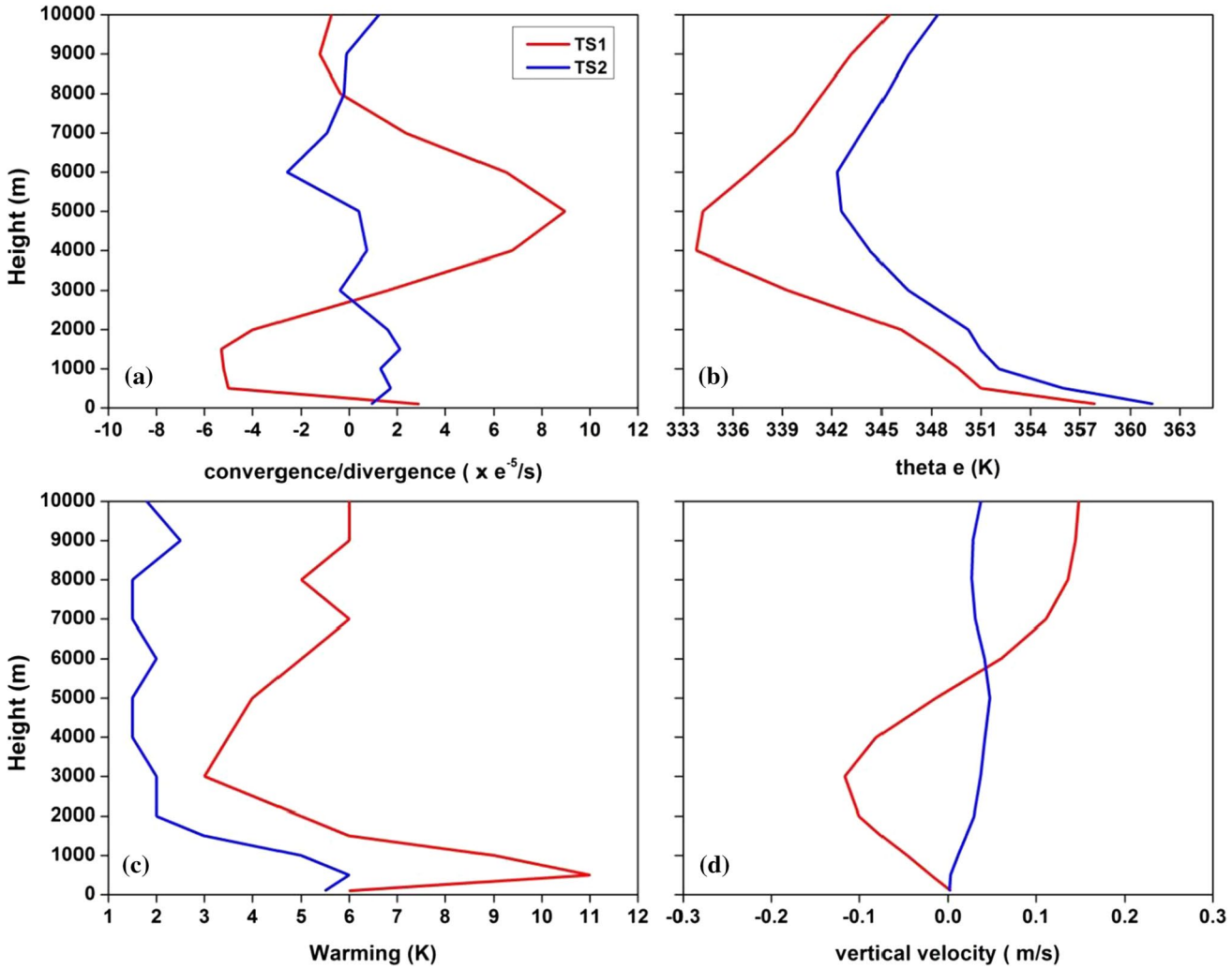

Fig. 15 Vertical profiles of area averaged (0.5×0.5 deg) convergence (**a**), theta-e (**b**), warming (**c**) and vertical velocity (**d**) for thunderstorms at Auroville and Chennai at 12 UTC/18 IST

to the development of stronger vertical winds (Das 1962). Wind shear is calculated in the lower layers from the surface to 700 hPa and in the upper atmosphere from 500 to 200 hPa. The time series of area-averaged wind shear in the lower and upper levels are presented in Fig. 16. We notice a substantial increase of wind shear from a low value of 4–5 m/s at 06UTC (12IST) to11 m/s at 12 UTC (18 IST) which shows a favorable condition in triggering the thunderstorm development (Fig. 16a) for TS1. The relatively high wind shear in the lower levels (11 m/s) and low wind shear in the upper levels (5 m/s) promotes vertical moisture transport by intense updrafts and the development of intense convection for the summer case. Though the monsoon event also shows the presence of considerable wind shear (10 m/s) in the lower atmosphere, the presence of high vertical wind shear (> 35 m/s) in the upper atmosphere does not promote intense updrafts/ convection which leads to moderately strong thunderstorms in monsoon period (Fig. 16b).

5.6 Vertical hydrometeors distribution

We compare the area average (0.1×0.1 deg) vertical distribution of simulated cloud hydrometeor mixing ratios of rain, cloud, snow and graupel (Fig. 17) around the storms to understand the differences in the cloud processes between the two cases. As shown in Fig. 17, large differences in the hydrometeor mixing rations can be seen. Both the simulations show a maximum concentration of rain in the lower layers (900–700 hPa), ice in the upper layers (300–100 hPa), snow in the middle -upper layers (700–300 hPa) and graupel in the middle layers (600–300 hPa). However, the summer event is marked by very large amounts of solid hydrometeors (ice, graupel, snow) in addition to the rainwater mixing ratio

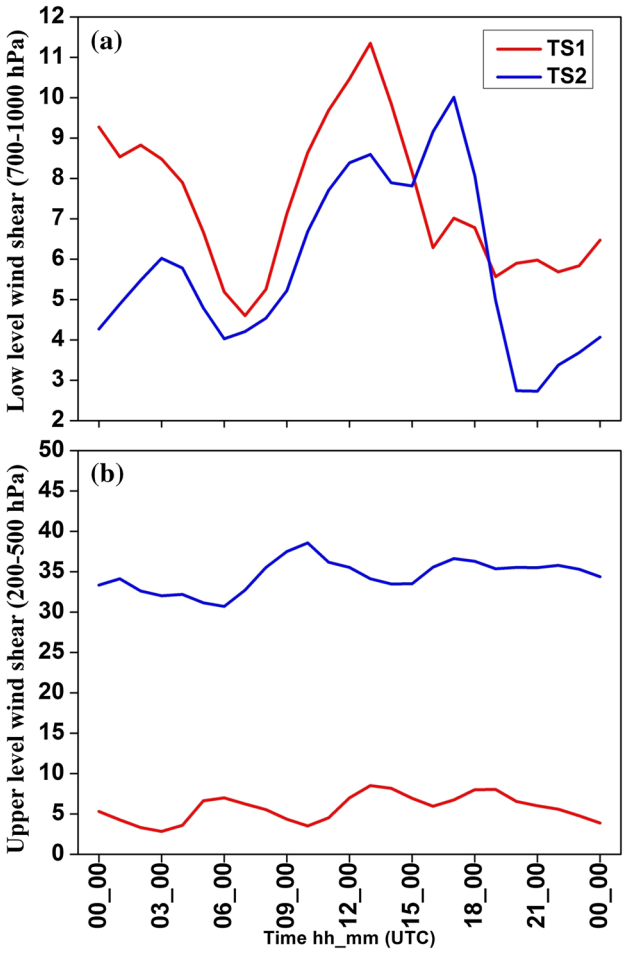

Fig. 16 Simulated area average (0.5×0.5 deg) wind shear at storm location (12.0° N and 79.5° E) for TS1 (in red) and (12.9° N and 80.1° E) for TS2 (in blue). Top panel (**a**) low-level (1000–700 hPa) wind shear and bottom panel (**b**) upper air (500–200 hPa) shear

indicating the role of stronger convection for the summer thunderstorm event.

6 Conclusions

This study examined the impact of sea breeze circulation on the development of convective thunderstorms over the southeast coast of India in different seasons using numerical simulations. Cloud-resolving simulations are conducted using the WRF-ARW model for two thunderstorms that occurred during the summer (24 April 2015) and monsoon period (22 July 2015). Simulations reveal that both the thunderstorm events developed in association with sea breeze convergence which is stronger in summer compared to the monsoon event. The convergence in the case of monsoon storms is less organized due to the relatively weak sea breeze flow compared to the summer events. Simulated storm characteristics (CAPE, convection, rainfall) varied according to the background flow and strength of the sea breeze which varied between summer and southwest monsoon periods. Simulations revealed the summer storm is relatively stronger compared to the monsoon event due to the development of more intense and deep sea breeze circulation cells and weak synoptic flow during summer. Both simulations and observations showed that the thunderstorm development during the summer season was early during the afternoon hours whereas it occurs in the late evening during the southwest monsoon. These differences are due to the variation in the synoptic flow condition, land-sea temperature contrast and the resulting differences in the sea breeze onset in the respective seasons. The thunderstorm event during monsoon is less intensive due to opposing large-scale monsoon flow which delayed the sea breeze propagation as well as its intensity leading to feeble convergence and convection. The relatively large surface energy and buoyancy fluxes in the boundary layer, high CAPE and low CIN for summer event indicate that the summer storm is associated with more unstable conditions than the monsoon storm case. A stronger vertical motion is found for the summer events and it is associated with a stronger convergence, higher buoyancy and higher CAPE compared to the monsoon events. Simulations showed stronger warming in response to stronger convergence, vertical motion, large moisture build-up and high theta-e in summer thunderstorms compared to monsoon event.

Simulations indicated that the low-level convergence along the sea breeze frontal zone and the presence of lower atmospheric wind shear during sea breeze are the main factors for the initiation of deep convection and intensification of the thunderstorms. Analysis of the simulations indicated that the low-level convergence and wind shear are stronger for the summer storm compared to the monsoon storm. The presence of stronger higher lower atmospheric wind shear (1000–700 hPa) and lower upper shear during summer favored the development of strong and deep convection compared to the monsoon event.

Simulations also showed that the presence of deep convection for summer thunderstorm events led to the development of deep convective clouds with higher vertical extent leading to more precipitation. Results showed that the simulated thunderstorms during summer are associated with more solid hydrometeors (ice, snow and graupel) due to deep convection compared to the monsoon season storms. The present study shows significant differences in various storm parameters between the summer and monsoon seasons. However, simulations with a greater number of cases along with observational analysis would be required for a better understanding of the seasonal characteristics of sea breeze-induced convective thunderstorms along the southeast coast of India.

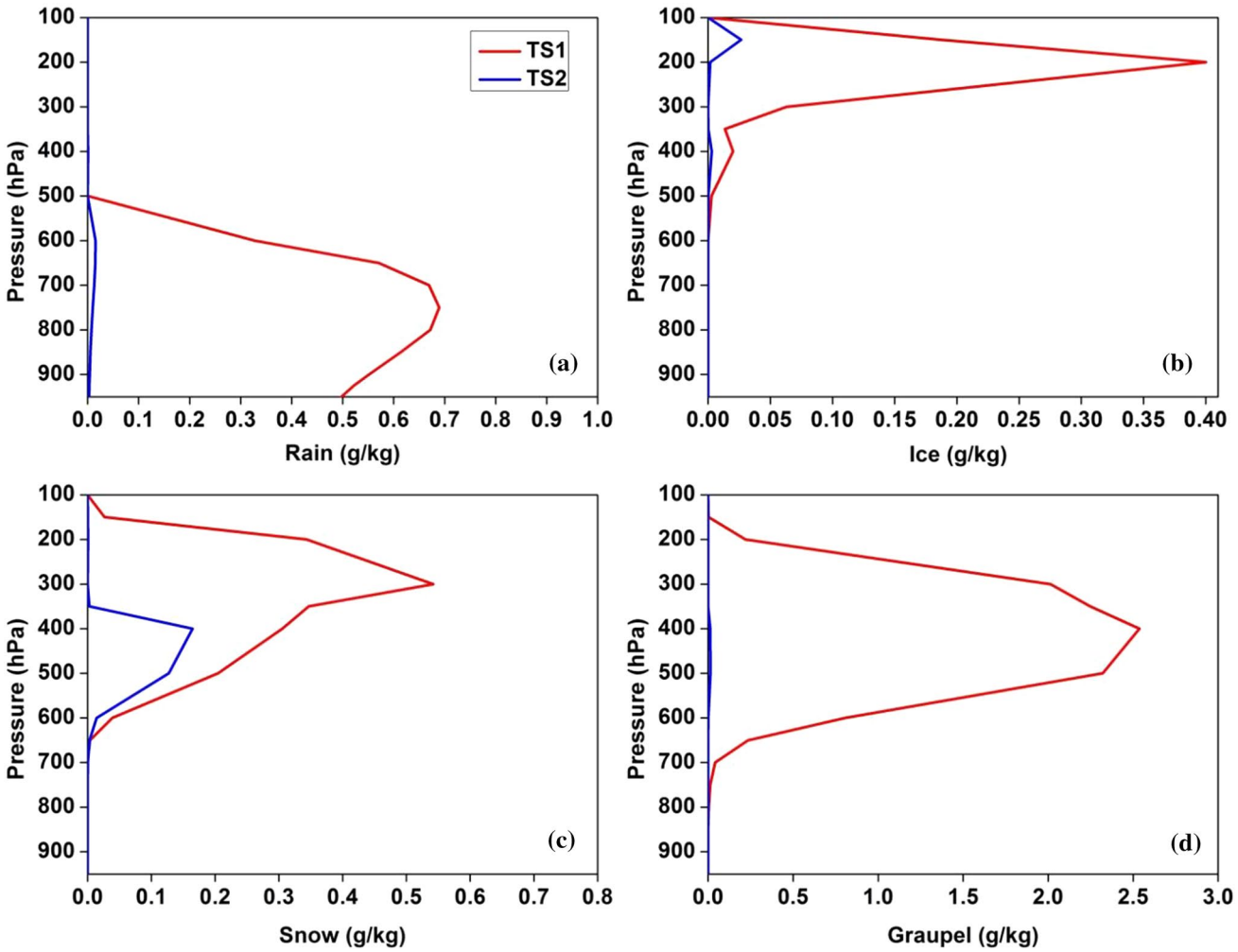

Fig. 17 Vertical profiles of mixing ratios of hydrometeors averaged over 0.1×0.1 deg **a** rain, **b** ice, **c** snow, **d** graupel at storm location (12.0° N and 79.5° E) for TS1 (in red) and (12.9 N and 80.1 E) for TS2 (in blue)

Acknowledgements Authors wish to thank Director, IGCAR, for the encouragement and support. The first author is grateful to HBNI for providing the research fellowship and IGCAR DAE for extending facilities to conduct the study. Authors acknowledge the India Meteorological Department for the access of DWR reflectivity data and the gridded rainfall observations used in the study. The Radiosonde observations of Chennai are accessed from the University of Wyoming. Authors thank MOSDAC-ISRO for the AWS observations used for the study. Authors wish to thank the anonymous reviewers for their technical comments which helped to improve the content of the paper.

References

Allen JT, Karoly DJ, Mills GA (2011) A severe thunderstorm climatology for Australia and associated thunderstorm environments. Aust Meteorol Oceanogr J 61:143–158

Arrillaga JA, Yague C, Sastre M, Roman-Cascon C (2016) A characterisation of sea-breeze events in the eastern Cantabrian coast (Spain) from observational data and WRF simulations. Atmos Res 181:265–280

Asnani GC (2005) Tropical Meteorology (Revised Edition).Indian Institute of Tropical Meteorology, Pune, 2

Azorín-Molina C, Chen D (2009) A climatological study of the influence of synoptic-scale flows on sea-breeze evolution in the Bay of Alicante (Spain). Theor Appl Climatol 96:249–260

Azorín-Molina C, Tijm S, Ebert ES, Vicente-Serrano Estrela M (2014) Sea breeze thunderstorms in the eastern Iberian Peninsula. Neighborhood verification of HIRLAM and HARMONIE precipitation forecasts. Atmos Res 139:101–115

Basu GC, Mondal DK (2002) A forecasting aspect of thundersquall over Calcutta and its parameterisation during pre-monsoon season. Mausam 53:271–280

Bhardwaj P, Singh O (2018) Spatial and temporal analysis of thunderstorm and rainfall activity over India. Atmósfera 31(3):255–284

Bhate J, Kesarkar AP, Karipot A, Subrahamanyam DB, Rajasekhar M, Sathiyamoorthy V, Kishtawal CM (2016) A sea breeze induced thunderstorm over an inland station over Indian south peninsula—a case study. J Atmos Sol Terr Phys 14:96–111

Calmet I, Mestayer PG, van Eijk AMJ, Herledant O (2017) A coastal bay summer breeze study, part 2: high-resolution numerical simulation of sea-breeze local influences. Boundary-Layer Meteorol. https://doi.org/10.1007/s10546-017-0319-1

Chappell CF, Smith DR (1975) Generation of the available buoyant energy by cloud glaciations. Pure Appl Geophys 113:825
Chaudhari HS, Sawaisarje GK, Ranalkar MR, Sen PN (2010) Thunderstorms over a tropical Indian station, Minicoy: role of vertical wind shear. J Earth Syst Sci 119(5):603–615
Chaudhuri SUTAPA, Bhowmick SA (2006) CAPE-A link amid thermodynamics and microphysics for the occurrence of severe thunderstorms. Mausam 57(2):249
Chen TC, Yen MC, Tsay JD, Liao CC, Takle ES (2014) Impact of afternoon thunderstorms on the land–sea breeze in the Taipei basin during summer: an experiment. J Appl Meteorol Climatol 53(7):1714–1738
Comin A, Miglietta M, Rizza U, Acevedo O, Degrazia G (2015) Investigation of sea-breeze convergence in Salento Peninsula (southeastern Italy). Atmos Res 160:68–79
Das P (1962) Influence of wind shear on the growth of hail. J Atmos Sci 19:407–414
Dinesh K, Mohanty UC, Krishan K (2016) Sensitivity of land surface and cumulus schemes for thunderstorm prediction. Int Arch Photogramm Remote Sens Spat Inf Sci 41
Dudhia J (1989) Numerical study of convection observed during the winter monsoon experiment using a mesoscale two-dimensional model. J Atmos Sci 46(20):3077–3107
Fadnavis S, Deshpande M, Ghude S, Raj P (2014) Simulation of severe thunder storm event: a case study over Pune, India. Nat Hazards 72:927–943
Fankhauser JC, Crook NA, Tuttle J, Miller LJ, Wade CG (1995) Initiation of deep convection along boundary layer convergence lines in a semitropical environment. Mon Weather Rev 123:291–313
Findlater J (1969) A major air current near the West Indian Ocean during the summer monsoon. Q J R Meteorol Soc 95:1251–1262
Garratt JR (1994) The atmospheric boundary layer. Earth Sci Rev 37(1–2):89–134. https://doi.org/10.1016/0012-8252(94)90026-4
Haklander AJ, Van Delden A (2003) Thunderstorm predictors and their forecast skill for the Netherlands. Atmos Res 67:273–299
Halder M, Mukhopadhyay P (2016) Microphysical processes and hydrometeor distributions associated with thunderstorms over India: WRF (cloud-resolving) simulations and validations using TRMM. Nat Hazard 83(2):1125–1155
Hariprasad KBRR, Srinivas CV, Bagavath Singh A, Vijaya Bhaskar Rao S, Baskaran R, Venkatraman B (2014) Numerical simulation and intercomparison of boundary layer structure with different PBL schemes in WRF using experimental observations at a tropical site. Atmos Res 145(146):27–44
Hari Prasad KBRR, Srinivas CV, Naidu CV, Baskaran R, Venkatraman B (2016) Assessment of surface layer parameterizations in ARW using micro-meteorological observations from a tropical station. MeteorolAppl 23(2):191–208
Hersbach H, Dee D (2016) ERA5 reanalysis is in production. ECMWF Newsletter 147(7), 5–6. Reading, UK: ECMWF
Hong SY, Noh Y, Dudhia J (2006) A new vertical diffusion package with an explicit treatment of entrainment processes. Mon Weather Rev 134:2318–3241
Kain JS, Fritsch JM (1993) Convective parameterization for mesoscale models: the Kain-Fritsch scheme. The representation of cumulus convection in numerical models. Amer Meteor Soc, Boston, MA, pp 165–170
Kandalgaonkar SS, Tinmaker MIR, Nath A, Kulkarni MK, Trimbake HK (2005) Study of thunderstorm and rainfall activity over the Indian region. Atmosfera 18(2):91–101
Kingsmill DE (1995) Convection initiation associated with a sea breeze front, a gust front, and their collision. Mon Weather Rev 123:2913–2933
Leena PP, Pandithurai G, Gayatri K, Murugavel P, Ruchith RD, Sakharam S, Dani KK, Patil C, Dharmaraj T, Patil MN, Prabhakaran T (2019) Analysing the characteristic features of a pre-monsoon thunderstorm event over Pune, India, using ground-based observations and WRF model. J Earth Syst Sci 128(4):1–15
Litta AJ, Mohanty UC (2008) Simulation of a severe thunderstorm event during the field experiment of STORM programme 2006, using WRF–NMM model. Current Science 204–215
Litta AJ, Mohanty UC, Idicula SM (2012) The diagnosis of severe thunderstorms with high-resolution WRF model. J Earth Syst Sci 121(2):297–316
Lutgens KF, Tarbuck JE (1982) Theatmosphere: an introduction to meteorology. Prentice-Hall, NJ, p 478
Mahrer Y, Pielke RA (1977) The effects of topography on sea and land breezes in a two-dimensional numerical model. Mon Weather Rev 105(9):1151–1162
Manohar GK, Kandalgaonkar SS, Tinmaker MIR (1999) Thunderstorm activity over India and the Indian southwest monsoon. J Geo Phy Res 104:4169–4188
Manzato A (2005) The use of sounding-derived indices for a neural network short-term thunderstorm forecast. Weather Forecast 20(6):896–917
Marion GR, Trapp RJ (2019) The dynamical coupling of convective updrafts, downdrafts, and cold pools in simulated supercell thunderstorms. J Geo Phy Res: Atmos 124:664–683
Mitra AK, Bohra AK, Rajeevan MN, Krishnamurti TN (2009) Daily Indian precipitation analysis formed from a merge of rain-gauge data with the TRMM TMPA satellite-derived rainfall estimates. J Meteor Soc Japan 87:265–279
Morrison H, Thompson G, Tatarskii V (2009) Impact of cloud microphysics on the development of trailing stratiform precipitation in a simulated squall line: comparison of one-and two-moment schemes. Mon Weather Rev 137(3):991–1007
Muppa S, Anandan V, Kesardar K, Rao S, Reddy P (2012) Study on deep inland penetration of sea breeze over complex terrain in the tropics. Atmos Res 104:209–216
Osuri KK, Nadimpalli R, Mohanty UC, Chen F, Rajeevan M, Niyogi D (2017) Improved prediction of severe thunderstorms over the Indian Monsoon region using high-resolution soil moisture and temperature initialization. Sci Rep 7(1):1–12
Poljak G, Prtenjak MT, Kvakić M, StrelecMahović N, Babić K (2014) Wind patterns associated with the development of daytime thunderstorms over Istria. Ann Geophys 32:401–420. https://doi.org/10.5194/angeo-32-401-2014
Prasad SK, Mohanty UC, Routray A, Osuri KK, Ramakrishna SSVS, Niyogi D (2014) Impact of Doppler weather radar data on thunderstorm simulation during STORM pilot phase—2009. Nat Hazards 74(3):1403–1427
Rajeswari JR, Srinivas CV, Rao TN, Venkatraman B (2020) Impact of land surface physics on the simulation of boundary layer characteristics at a tropical coastal station. Atmos Res 238:104888
Rani SI, Ramachandran R, Subrahamanyam DB, Alappattu DP, Kunhikrishnan PK (2010) Characterization of sea/land breeze circulation along the west coast of Indian sub-continent during premonsoon season. Atmos Res 95(4):367–378
Reshmi Mohan P, Srinivas CV, Yesubabu V, Baskaran R, Venkatraman B (2018) Simulation of a heavy rainfall event over Chennai in southeast India using WRF: sensitivity to microphysics parameterization. Atmos Res 210:83–99
Reshmi Mohan P, Srinivas CV, Yesubabu V, Baskaran R, Venkatraman B (2019) Tropical cyclone simulations over Bay of Bengal with ARW model: Sensitivity to cloud microphysics schemes. Atmos Res 230:104651
Revanth Reddy B, Srinivas CV, Shekhar SR, Baskaran R, Venkatraman B (2020) Impact of land surface physics in WRF on the simulation of sea breeze circulation over southeast coast of India. Meteorol Atmos Phys 13:1–9
Revanth Reddy B, Srinivas CV, Venkatraman B (2022) Observational analysis and numerical simulation of sea breeze using WRF model

over the Indian southeast coastal region. Meteorol Atmos Phys 134:57

Sahu RK, Dadich J, Tyagi B, Vissa NK (2020) Trends of thermodynamic indices thresholds over two tropical stations of north-east India during pre-monsoon thunderstorms. J Atmos Solar Terrestrial Phys 211:105472

Schlemmer L, Hohenegger C (2014) The formation of wider and deeper clouds as a result of cold pool dynamics. J Atmos Sci 71(8):2842–2858

Shepherd JM, Ferrier BS, Ray PS (2001) Rainfall Morphology in Florida convergence zones: a numerical study. Mon Weather Rev 129:177–197

Simpson M, Warrior H, Raman S, Aswathanarayana PA, Mohanty UC, Suresh R (2007) Sea-breeze-initiated rainfall over the east coast of India during the Indian southwest monsoon. Nat Hazards 42(2):401–413

Simpson M, Raman S, Suresh R, Mohanty UC (2008) Urban effects of Chennai on sea breeze induced convection and precipitation. J Earth Sys Sci 117(6):897–909

Sindhu KD, Bhat GS (2021) Seasonal characteristics of storms over the Indian subcontinent. Sci Rep 11:3355. https://doi.org/10.1038/s41598-021-82237-w

Singh J, Gairola A, Das S (2015) Numerical simulation of a severe thunderstorm over Delhi Using WRF Model. Int J Sci Res Publications 5(6):327–332

Sisodiya A, Pattnaik S, Baisya H, Bhat GS, Turner AG (2019) Simulation of location-specific severe thunderstorm events using high resolution land data assimilation. Dyn Atmos Oceans 87:101098

Srikanth M, Satyanarayana ANV, Srinivas CV, Tyagi B (2016a) Performance evaluation of PBL schemes of ARW model in simulating thermo-dynamical structure of pre-monsoon convective episodes over Kharagpur using STORM data sets. Pure Appl Geophys 173(5):1803–1827

Srikanth M, Hari Prasad KBRR, Srinivas CV, Satyanarayana ANV (2016b) Air quality simulation of NOX over the tropical coastal city Chennai in southern India with FLEXPART-WRF. Atmos Environ 128:65–81

Srikanth M, Srinivas CV, Satyanarayana ANV (2018) Performance of WRF for simulation of mesoscale meteorological characteristics for air quality assessment over Tropical Coastal City, Chennai. Pure Appl Geophys 175(1):501–518

Srinivas CV, Venkatesan R, Somayaji KM, BagavathSingh A (2006) A numerical study of sea breeze circulation observed at a tropical site Kalpakkam on the east coast of India, under different synoptic flow situations. J Earth Sys Sci 115(5):557–574

Srinivas CV, Hariprasad KBRR, Naidu CV, Baskaran R, Venkatraman B (2016) Sensitivity analysis of atmospheric dispersion simulations by FLEXPART to the WRF simulated meteorological predictions in a coastal environment. Pure Appl Geophys 173:675–700

Srivastava K, Bhowmik SR, Hatwar HR, Das AK, Kumar A (2008) Simulation of mesoscale structure of thunderstorm using ARPS model. Mausam 59(1):1–14

Srivastava K, Roy Bhowmik SK, Sen Roy S, Thampi SB, Reddy YK (2010) Simulation of high impact convective events over Indian region by ARPS model with assimilation of Doppler weather radar radial velocity and reflectivity. Atmosfera 23(1):53–73

Suresh R (2012) Forecasting and nowcasting convective weather phenomena over southern peninsular India - Part-I: thunderstorm. Indian J Radio Space Phy 41:421–434

Suresh R, Bhatnagar AK (2005) Pre-convective environment of pre-monsoon thunderstorms around Chennai- a thermodynamical study. Mausum 56:659–670

Tyagi A (2007) Thunderstorm climatology over Indian region. Mausum 58:189–212

Viswanadhapalli Y, Dasari HP, Dwivedi S, MadineniVR LS, Hoteit I (2019) Variability of monsoon low level jet and associated rainfall over India. Int J Climatol 40(2):1067–1089

Wallace JM, Hobbs RV (1977) Atmospheric science: an introductory survey. Academic, NY, p 467

Xavier A, Kottayil A, Mohanakumar K, Xavier PK (2017) The role of monsoon low-level jet in modulating heavy rainfall events. Int J Climatol 38:569–576

Zhao Y, Chen D, Li J, Chen D, Chang Y, Li J, Qin R (2020) Enhancement of the summer extreme precipitation over north China by interactions between moisture convergence and topographic settings. Clim Dyn 54:2713–2730